Frontiers in Bioscience Landmark

Front. Biosci. (Landmark Ed) **2023**; 28(5): 87
https://doi.org/10.31083/j.fbl2805087

Original Research

Dynamics of Chronic Liver Injury in Experimental Models of Hepatotoxicity

Piotr Czekaj[1,*,†], Mateusz Król[1,†], Emanuel Kolanko[1], Łukasz Limanówka[2], Agnieszka Prusek[1], Aleksandra Skubis-Sikora[1], Edyta Bogunia[1], Bartosz Sikora[1], Mateusz Hermyt[1], Marcin Michalik[1], Aniela Grajoszek[3], Jacek Pająk[4]

[1]Department of Cytophysiology, Chair of Histology and Embryology, Faculty of Medical Sciences in Katowice, Medical University of Silesia in Katowice, 40-752 Katowice, Poland
[2]Students Scientific Society, Chair of Histology and Embryology, Faculty of Medical Sciences in Katowice, Medical University of Silesia in Katowice, 40-752 Katowice, Poland
[3]Department of Experimental Medicine, Medical University of Silesia in Katowice, 40-752 Katowice, Poland
[4]Department of Pathomorphology and Molecular Diagnostic, Faculty of Medical Sciences in Katowice, Medical University of Silesia in Katowice, 40-752 Katowice, Poland
*Correspondence: pcz@sum.edu.pl (Piotr Czekaj)
[†]These authors contributed equally.
Academic Editor: Rolf Teschke
Submitted: 1 February 2023 Revised: 7 April 2023 Accepted: 27 April 2023 Published: 9 May 2023

Abstract

Background: In humans, chronic liver disease (CLD) is a serious clinical condition with many life-threatening complications. Currently, there is no therapy to stop or slow down the progression of liver fibrosis. Experimental mouse models of CLD, induced by repeated intraperitoneal injections of carbon tetrachloride (CCL_4) and D-galactosamine (D-GalN), can be used to evaluate therapies that cannot be performed in humans. A major drawback of these animal models is the different dynamics of liver fibrosis progression depending on the animal strain, administered hepatotoxin, its dose, duration of intoxication, and frequency of injections. The aim of this study was to describe and compare the dynamics of progression of pathological changes in the BALB/c mouse and Sprague Dawley rat models of CLD induced by CCl_4 and D-GalN. We defined the onset and duration of these changes and suggested the optimal time for therapeutic intervention in the analyzed CLD models. **Methods**: CLD was induced by repeated intraperitoneal injection of CCl_4 in mice (12.5 μL/100 g bw every 5 days) and rats (25–100 μL/100 g bw twice a week) and D-GalN in mice (75 mg/100 g bw twice a week) and rats (25 mg/100 g bw twice a week). Blood and liver samples were collected at weeks 2, 4, 6, 8, 10, and 12 of intoxication. Liver injury and its progression were assessed by using complete blood count and liver function blood tests as well as by analyzing histopathological changes, including fibrosis, proliferation activity, apoptosis, stellate cell activation, and gene expression. **Results**: In mice and rats treated with CCl_4, early fibrosis was observed in most pericentral areas from week 2 to 4 of intoxication. Established fibrosis developed in both rats and mice at week 6 of intoxication. Incomplete cirrhosis, defined as the presence of occasional cirrhotic nodules, was observed in rats at week 12 of intoxication. The dynamics of liver fibrosis in CCl_4-treated animals were greater than in the D-GalN groups. In D-GalN-intoxicated rats and mice, the first signs of liver fibrosis were observed at weeks 4 and 10 of intoxication, respectively. The rats developed early fibrosis after 8 weeks of D-GalN intoxication. The progression of collagen deposition was accompanied by histological changes and alteration of certain genes and blood liver parameters. **Conclusions**: The dynamics of liver fibrosis in CCl_4 treated rodents is greater than in the D-GalN treated ones. In the CCl_4 models, two appropriate times for therapeutic intervention are indicated, which to varying degrees reflect the real clinical situation and may potentially differ in the obtained results: early intervention before week 4 of intoxication (early fibrosis) and late intervention after week 8 of intoxication (when signs of established fibrosis are present). Rodent models of D-GalN-induced fibrosis are not recommended due to the long incubation period and weak toxic effect.

Keywords: experimental models of hepatotoxicity; galactosoamine; carbon tetrachloride; chronic liver failure; stem cell therapy

1. Introduction

In humans, chronic liver disease (CLD) is a large group of clinical conditions characterized by impairment of liver function and morphology lasting over 6 months. The most common causes of CLD are alcohol consumption and viral infection. Less common etiological factors of CLD include nonalcoholic steatohepatitis, biliary obstructive disorders, right sided heart failure, Wilson's disease, hemochromatosis, and chronic use of specific medications [1]. Regardless of the etiology, untreated CLD leads to cirrhosis, which is defined as pathological remodeling of the liver parenchyma with fibrotic scar formation and presence of regenerative nodules. The pathogenesis of this disease involves the destruction of parenchymal cells by the causative agent. Apoptosis or necrosis of hepatocytes induces an inflammatory reaction that activates hepatic stellate cells (HSCs) via multiple cytokines such as IGF-1, TGF-α, and EGF. Activated HSCs differentiate into myofi-

Table 1. Course of intraperitoneal injections in rats and mice. Animals in the experimental groups received hepatotoxin solvents at the same volume as control rats and mice injected with hepatotoxin solutions, saline, or olive oil.

Hepatotoxin	Control groups		Chronic liver injury	
	Rats	Mice	Rats	Mice
Carbon tetrachloride	200 μL/100 g olive oil bw (0–2 week); 100 μL/100 g bw (2–4 week); 50 μL/100 g bw (4–12 week); twice a week	25 μL olive oil, every fifth day	100 μL/100 g bw (0–2 week); 50 μL/100 g bw (2–4 week); 25 μL/100 g bw (4–12 week); twice a week	12.5 μL/100 g bw; every fifth day
D-GalN hydrochloride	250 μL/100 g saline, twice a week	125 μL/100 g saline, twice a week	25 mg/100 g bw, twice a week	75 mg/100 g bw; twice a week

broblasts, which secrete large amount of collagen and extracellular matrix (ECM) components into the space of Disse [2]. CLD often shows no signs or symptoms. At a later stage of the disease, signs and symptoms result from decreased parenchymal cell volume (e.g., hypoalbuminemia, coagulopathy, encephalopathy, jaundice) or portal hypertension (e.g., ascites, esophageal varices) caused by collagen deposition in perisinusoidal spaces. The primary treatment for CLD is withdrawal of the causative agent (alcohol, medications) or treatment of the underlying disease (viral infection, biliary obstructive disorders). At an early stage of cirrhosis, treatment involves dietary and electrolyte therapy, blood component transfusions, antibiotic therapy, and administration of drugs reducing portal hypertension (β-blockers, simvastatin). In cases of complications such as bleeding from esophageal varices, additional life-saving surgical procedures are needed [3]. When signs and symptoms of CLD are severe and the patient meets the appropriate Child-Pugh score criteria, the only effective therapeutic option is liver transplantation. However, organ transplantation has important drawbacks including high cost, low organ availability, the need for lifelong immunosuppression therapy, and risk of multiple complications [4–6]. Therefore, it is imperative to develop an effective therapy that will be able to slow down or even stop fibrosis progression to avoid the need for liver transplantation. Stem cell-based therapies could potentially slow down fibrosis by inhibiting the inflammatory reaction [7,8].

Animal models of hepatotoxicity induced by hepatotoxins, including carbon tetrachloride (CCl_4) and D-galactosamine (D-GalN), can be used in preclinical assessment of CLD therapies. Such models allow for long-term observation that cannot be performed in patients for ethical and medical reasons, particularly observation of the progression of liver diseases [9,10] characterized by fibrosis, as well as assessment of the efficacy and safety of an advanced therapy. Unfortunately, the various mechanisms of xenobiotic toxicity and the different sensitivity of animal species and strains to intoxication result in different intoxication effects and, consequently, some difficulties in interpreting the data and extrapolating them to humans [10]. To induce fibrosis in mice and rats, the CCl_4 dose should be 10–200 μL per 100 g bw, administered two to three times a week. Fibrosis incubation time varies by protocol and is usually between 4 and 12 weeks. To induce cirrhosis, incubation time should be extended to 12–20 weeks. The ability of D-GalN to induce cirrhosis is questionable. Compared to CCl_4, D-GalN causes less severe inflammatory reaction, and thus D-GalN has lower potency to induce fibrosis. To induce fibrosis in mice and rats, the D-GalN dose should be 50–150 mg/100 g bw and 25–50 mg/100 g bw, respectively, and the period of exposure to this hepatotoxin should be at least 12 weeks. Despite the above-mentioned drawbacks, D-GalN intoxication better histopathologically mimics human viral infection compared to CCl_4.

In the present study, we compared the development of histopathological changes induced in Sprague Dawley rat and BALB/c mouse experimental models by repeated injections of CCl_4 and D-GalN at doses and frequencies described as effective [11–14]. We analyzed the usefulness of these models with a view to their future introduction into preclinical experiments. In particular, based on histopathological and molecular changes it allowed us to identify potential experimental time cut-off points when pharmaceutical or stem cell therapeutic intervention might be effective. So far, the effectiveness of antifibrotic cell therapy has been proven in animal models using primary hepatocytes, mesenchymal stem cells (MSCs) [15–17], and embryonic stem cells (ESCs) [18]. Recently, a novel cell therapy using immunomodulatory human amniotic cells (hAC) has been proposed [7,19–23].

2. Material and Methods

2.1 Animals

The study was performed on two-month-old male Sprague Dawley rats weighing 180–220 g, and six-week-old male BALB/c mice weighing 18–25 g, purchased from the Animal House of the Center for Experimental Medicine (CMD) of the Medical University of Silesia in Katowice. During the experiment, the animals were housed in cages (six per cage) under standard conditions of temperature (22 °C $\pm$ 2 °C), humidity (50–60%), light/dark cycle (12 h/12 h), and light intensity (60–400 lux) with ad libitum access to water and standard laboratory chow (Labofeed). Animals were not fasted during the experiment.

The study was approved by the Local Ethics Committee for Animal Experiments of the Medical University of Silesia (decision no. 18/2018). Rats and mice were treated in accordance with the Directive 2010/63/EU on animal experimentation.

2.2 Experimental Design

The animals were randomly divided into 4 groups (18 individuals per group). D-galactosamine hydrochloride (no. 22981; Cayman Chemical; Ann Arbor, Michigan, USA) was dissolved in physiological saline. Carbon tetrachloride (no. 118804704; Chempur; Piekary Śląskie, Poland) was diluted 1:1 in olive oil (Sigma-Aldrich; St.Louis, MI, USA). The xenobiotics were administered intraperitoneally (i.p.) at the doses shown in Table 1. At each of the scheduled time points (weeks 2, 4, 6, 8, 10, and 12), three days after the last xenobiotic injection, three animals per group were anaesthetized by i.p. injection of 100 mg/kg ketamine and 10 mg/kg xylazine and sacrificed. Blood and tissue samples were taken on the day of anesthesia. Samples from the control groups were collected at the same time, three days after the last saline or oil injection.

2.3 Blood Tests

During autopsy, 1 mL of orbital sinus blood was collected. Alanine transaminase (ALT), aspartate transaminase (AST), and alkaline phosphatase (ALP) activities and total protein (TP) were measured to assess liver injury by liver function tests. Blood tests were performed on a chemistry analyzer (AU480; Beckman Coulter, Brea, CA, USA) according to protocols provided by the manufacturer. In addition, blood smears stained with May Grunwald-Giemsa stain were done to assess cell morphology. Serum biochemistry tests and blood staining were performed in the Silesian Analytical Laboratory (Katowice; Poland).

2.4 Histopathological Analysis

The excised sections of the left liver lobe were fixed in 10% buffered formalin solution, dehydrated, and embedded in paraffin. The obtained paraffin blocks were cut into 4 μm sections, which were then deparaffinized, rehydrated, and stained with hematoxylin and eosin (H&E) by standard procedure.

The severity of hepatitis was assessed by a simple grading algorithm evaluating parenchymal injury and interface hepatitis. Normal liver parenchyma was graded as (0). Hepatitis was graded as follows: minimal (1), mild (2), moderate (3), and marked and/or multiacinar bridging necrosis (4) [24,25]. Liver steatosis was graded as follows: $<$5% (none; 0), 5–33% (mild; 1), 34–66% (moderate; 2), and $>$67% (severe; 3) [26].

The progression of liver fibrosis was evaluated by Sirius red staining, which was performed to visualize collagen fibers. Liver sections (4 μm-thick) were dewaxed, rehydrated, and incubated with Weigert's hematoxylin for 8 min and with picrosirius red in saturated picric acid for 60 min. Finally, they were washed thoroughly with acetic acid and water, covered, and examined under polarized light (microscope BX-43; Olympus, Tokyo, Japan). Observation of liver sections stained with Sirius red under polarized light allows for accurate calculation of collagen fiber content and assessment of fiber thickness. The 'color' of the stained collagen fibers under polarized light corresponds to their thickness. In this observation technique, thick collagen fibers appear red and orange, while thin fibers appear yellow and green.

To quantify the percentage area occupied by collagen fibers, fifteen random fields of 0.0944 mm^2 from each slide were photographed at 200$\times$ magnification and analyzed using ImageJ analysis software (US National Institutes of Health; Bethesda, MD, USA) [27] and the Ishak semi-quantitative scoring system [28,29]. Moreover, the thickness of collagen fibers was evaluated under polarized light using the protocol described by Rich and Whittaker [30].

2.5 Immunohistochemistry

The localization of cells expressing Ki-67, a marker of proliferation, α-SMA, a marker of HSC activation, and activated caspase-3, a marker of apoptosis, was visualized immunohistochemically in deparaffinized 4-μm-thick rat and mouse liver sections. To quench the endogenous peroxidase activity, the sections were blocked with 3% H_2O_2 for 10 min. Mouse IgG served as an isotype-matched negative control.

Before incubation with the primary antibody, the sections intended for Ki-67 visualization were incubated for 60 min with a citric acid-based antigen unmasking solution (Vector Laboratories; Newark, CA, USA) for antigen retrieval. Non-specific antibody binding was then blocked using 2.5% equine serum (Vector Laboratories; Newark, CA, USA) for 60 min. Subsequently, liver sections were incubated with anti-Ki67 (SP6) antibody (ab16667; Abcam, Cambridge, United Kingdom) diluted 1:400 for 20 h at 4 °C and with anti-rabbit secondary antibody conjugated with peroxidase (Vector Laboratories; Newark, CA, USA) at room temperature for 30 min. Appropriate positive controls were created as sections taken from human tonsils.

Liver sections intended for identifying apoptotic cells and, separately, alpha-smooth muscle actin (α-SMA) were incubated with a citric acid-based antigen unmasking solution (Vector Laboratories Newark, CA, USA) for 30 min. Then, they were pretreated with 5% goat serum (Vector Laboratories; Newark, CA, USA) to block non-specific antibody binding sites. This stage was followed by incubation with cleaved Cas-3 (#9661; Cell Signaling; MA, USA) diluted 1:500 for 20 h at 4 °C or with α-SMA antibody (ab5694; Abcam, Cambridge, United Kingdom) diluted 1:2000 for 20 h at 4 °C. Next, liver slices were incubated with an anti-rabbit secondary antibody (Cell Signal-

Table 2. List of genes evaluated in the study.

Gene name	Gene abbreviation	Function	References
Type I collagen	*COL1A1*	Liver fibrosis	[32]
Type III collagen	*COL3A1*		
Transforming growth factor beta	*TGF-β*		
Tyrosine-protein kinase Met	*c-Met*	Angiogenesis	[33,34]
Hepatocyte growth factor	*HGF*		
Cytochrome P450 2E1	*CYP2E1*	Oxidative stress	[35]
Peroxisome proliferator-activated receptor alpha	*PPAR-α*	Lipid metabolism	[36]
Growth arrest and DNA-damage-inducible protein alpha	*Gadd45a*	Carcinogenesis	[37]

ing; MA, USA) at 4 °C for 30 min and at room temperature for 30 min.

Final visualization was achieved by using diaminobenzidine (Vector Laboratories; Newark, CA, USA). On each slide, ten random fields of 0.3779 mm^2 each were photographed at magnifications of 100× and 200×. The data were analyzed using ImageJ software and expressed as the mean number of positive cells per field of interest (Ki67), percentage of positive area per field of interest (α-SMA), or on a semi-quantitative scale (Cas3). To quantify α-SMA^+ stellate cells, arterial and venous vascular walls were excluded from the computer evaluation because of positive staining in smooth muscle cells. The analysis of cleaved caspase-3 immunoreactivity in CCl_4- and D-GalN-induced apoptosis used the following semi-quantitative scale: (0) no positive cells; (1) few (<10) positive cells per field; (2) 10–25 positive cells per field; (3) 25–50 positive cells per field; (4) >50 positive cells per field and/or clusters of apoptotic cells. The repeatability of this scoring method was assessed by evaluating intra- and inter-observer correlations. Intra-observer repeatability was substantial (κ = 0.68), and inter-observer repeatability was moderate (κ = 0.43). A semi-quantitative scale was constructed according to previous recommendations [31].

2.6 Quantitative Real-Time Polymerase Chain Reaction

Small sections taken from the liver were homogenized using a Unidrive X 1000 homogenizer (CAT, Ballrechten-Dottingen, Germany). Total cellular RNA was isolated using the commercially available RNA Extracol reagent (Eurx, Gdańsk, Poland) according to the manufacturer's instructions. Nucleic acid concentration and quality were measured with Nanodrop ND-2000 (Thermo Scientific, Waltham, MA, USA). RNA was stained with Simply Safe (Eurx, Gdańsk, Poland) and visualized after agarose gel electrophoresis.

Ribonucleic acid was reverse-transcribed into complementary deoxyribonucleic acid (cDNA) using total RNA and random hexamer primers of the smART First Strand cDNA Synthesis Kit (Eurx, Gdańsk, Poland) and β-actin (ACTB) reference gene according to the manufacturer's instructions. The reference gene was selected as an endogenous positive control in separate qPCR among *HPRT1*, *TFRC*, *ACTB*, *TBP*, and *PPIH* genes for rat samples and among *HPRT1*, *ACTB*, *GUSB*, and *PPIH* genes for mouse samples.

The expression of eight genes involved in liver fibrosis, angiogenesis, oxidative stress, lipid metabolism, and carcinogenesis (Table 2, Ref. [32–37]) was detected using FastStart Essential DNA Green Master (Roche, Basel, Switzerland) in Light Cycler 96 (Roche, Basel, Switzerland). All samples were tested in triplicate. The oligonucleotide primers used in the reactions were purchased from Sigma Aldrich Company (St.Louis, MO, USA). Each run was completed using melting curve analysis to confirm the specificity of the amplification and absence of primer dimers. The relative expression of the examined genes was calculated according to the $2^{-\Delta Ct}$ method.

2.7 Statistical Analysis

The data was analyzed using the Statistica 13 computer software (StatSoft Polska, Kraków, Poland). Parametric analysis of the obtained results was performed using one-way ANOVA with appropriate post-hoc tests. The Kruskal-Wallis test was used if normal distribution could not be assumed. For independent groups, Student's *t*-test was also used where appropriate. Differences were considered as significant if $p < 0.05$.

3. Results

3.1 Blood Smears and Serum Biochemistry

In rats intoxicated with CCl_4, we observed a decrease in the number of lymphocytes and an increase in the number of monocytes and segmented neutrophils in week 2 after intoxication ($p < 0.05$). The percentage of leukocytes also showed a downward trend at week 12. In CCl_4-treated rats, there were no additional significant changes in the percentage of blood cells after repeated hepatotoxin injections. Also in the group of rats D-GalN-intoxicated rats, changes in blood cell counts were limited compared to D-GalN-treated mice and were observed only at week 2 (Table 3).

Changes in the percentage of blood cells in the group of CCl_4 injected mice were much more pronounced than in rats and varied at different time points (Table 3). There was no clear upward or downward trend after repeated CCl_4 administration over 12 weeks. In D-GalN-intoxicated mice,

Table 3. Percentage of blood cells found in routine smears taken from rats and mice intoxicated with CCl_4 and D-GalN.

Time point	Leukocytes [$10^3/\mu L$]	Lymphocytes [%]	Monocytes [%]	Eosinophils [%]	Band neutrophils [%]	Segmented neutrophils [%]
	Carbon Tetrachloride Rats					
Control	5.0 (3.0–5.2)	74 (67–79)	0 (0–0)	0 (0–2)	1 (0–3)	20 (15–25)
2 w	6.9 (6.8–7.0)	53 (50–55)*	2 (1–2)*	0 (0–0)	1 (0–2)	45 (43–47)*
4 w	6.2 (4.8–7.5)	77 (69–85)	0 (0–0)	2 (1–2)	2 (1–3)	20 (12–27)
6 w	5.5 (5.0–9.0)	67 (59–77)	0 (0–0)	1 (1–2)	1 (1–3)	31 (20–37)
8 w	6.0 (5.2–10.5)	73 (28–84)	0 (0–0)	0 (0–1)	2 (0–3)	26 (14–69)
10 w	6.0 (2.3–6.7)	54 (21–75)	0 (0–1)	2 (0–2)	1 (0–4)	43 (18–79)
12 w	1.7 (1.5–1.8)	76 (76–76)	0 (0–0)	2 (1–2)	3 (2–3)	20 (19–21)
	Carbon Tetrachloride Mice					
Control	4.5 (3.8–5.0)	46 (42–47)	0 (0–2)	0 (0–1)	0 (0–1)	53 (50–58)
2 w	5.6 (4.5–6.7)	19 (11–26)*	5 (1–9)	2 (0–3)	2 (1–2)	74 (68–79)*
4 w	3.4 (2.3–4.5)	61 (59–62)*	0 (0–0)	1 (0–1)	0 (0–0)	39 (37–41)*
6 w	3.8 (1.8–6.0)	44 (33–50)	1 (0–2)	0 (0–0)	0 (0–0)	55 (48–67)
8 w	4.8 (4.5–5.0)	44 (42–46)	1 (0–1)	0 (0–0)	0 (0–0)	56 (53–58)
10 w	15.0 (12.0–18.0)*	22 (18–24)*	4 (4–5)*	0 (0–0)	0 (0–1)	74 (72–76)*
12 w	4.5 (3.0–7.5)	50 (34–56)	2 (2–6)	0 (0–0)	0 (0–0)	48 (42–60)*
	D–Galactosamine Rats					
Control	2.5 (2.2–4.0)	78 (76–88)	0 (0–0)	2 (2–6)	2 (0–5)	15 (8–18)
2 w	6.0 (5.8–8.5)*	66 (64–71)*	0 (0–1)	2 (0–3)	1 (0–3)	31 (26–33)*
4 w	4.5 (3.5–7.5)	78 (72–81)	0 (0–0)	1 (0–2)	1 (0–3)	21 (16–25)
6 w	3.8 (3.0–4.0)	79 (67–90)	0 (0–0)	1 (1–7)	1 (1–1)	18 (8–25)
8 w	4.0 (3.0–5.7)	86 (74–88)	0 (0–0)	1 (1–2)	2 (0–2)	11 (8–25)
10 w	4.2 (2.5–4.8)	74 (45–75)	0 (0–1)	3 (1–4)	1 (0–1)	24 (22–49)
12 w	4.6 (3.8–5.3)	78 (70–86)	0 (0–0)	4 (1–7)	2 (2–2)	16 (11–21)
	D–Galactosamine Mice					
Control	4.5 (4.5–4.5)	62 (48–62)	3 (0–4)	0 (0–2)	0 (0–1)	38 (31–49)
2 w	6.0 (3.8–12.0)	57 (54–64)	1 (0–3)	1 (0–1)	0 (0–3)	36 (36–44)
4 w	2.5 (2.0–3.0)*	71 (70–93)	0 (0–1)	0 (0–0)	0 (0–1)	29 (6–29)
6 w	2.5 (2.4–4.5)	66 (61–74)	0 (0–0)	0 (0–0)	0 (0–0)	34 (26–39)
8 w	2.2 (1.8–2.5*	71 (67–75)	0 (0–0)	1 (0–1)	1 (0–1)	29 (25–31)
10 w	4.5 (3.0–6.0)	51 (49–58)	0 (0–0)	0 (0–0)	0 (0–0)	49 (42–51)
12 w	5.5 (5.0–6.0)*	67 (53–74)	1 (1–2)	0 (0–0)	1 (0–2)	31 (22–46)

Data are presented as a median (min-max). No basophils were identified in blood smears; n = 3. *$p < 0.05$, statistically significant as compared to controls.

the only change was a decrease in total leukocyte count observed between weeks 4 and 8 of observation (Table 3).

The obtained data indicate that there are only minor changes in the percentage of white blood cells, caused by long-term administration of CCl_4 and D-GalN. These changes do not show a discernible pattern.

We did not observe significant changes in ALT and AST activities in rats and mice intoxicated with CCl_4 and D-GalN between weeks 2 and 12. Elevated values of ALT and AST activities occurred in CCl_4-treated mice at some time points (i.e., in weeks 6, 8, and 10) but these changes were not statistically significant. There was a more pronounced increase in ALP values in CCl_4-treated mice between weeks 4 and 12 ($p < 0.05$) (Table 4).

Similarly to blood smears, we did not observe a clear pattern of long-term changes in serum parameters, reflecting toxic effects of both toxic compounds.

3.2 Histopathological Findings

Most CCl_4-treated rats developed mild or moderate liver steatosis. Hepatocytes containing lipid droplets were localized around the central veins (zone 3 of hepatic acini), both at early (weeks 2 and 4) and late (weeks 8, 10, and 12) time points. Other histopathological changes, namely minimal hepatitis, including parenchyma congestion, hepatocyte degeneration, and lymphocyte infiltration, were observed from week 4 of intoxication (Fig. 1, Table 5).

In mice treated with CCl_4, we did not observe liver steatosis during 12 weeks of observation. We observed minor ballooning degeneration around the central veins from weeks 2 to 6 of intoxication, followed by moderate hepatitis with spotty necrosis at week 8. Severe changes in the

Table 4. Changes in the serum parameters of rats and mice intoxicated with CCl_4 and D-GalN.

Time point	Alanine transaminase (ALT) [U/L]	Aspartate transaminase (AST) [U/L]	Alkaline phosphatase (ALP) [U/L]	Total Protein [g/dL]
	Carbon Tetrachloride Rats			
Control	50.7 (49.3–66.2)	201.6 (131.4–260.4)	229.5 (172.5–289.4)	6.2 (5.7–6.3)
2 w	106.4 (84.8–128)	254.25 (230.3–278.2)	234.05 (194.4–273.7)	6 (5.8–6.2)
4 w	96.1 (78.4–113.8)	197.9 (197.6–198.2)	320.75 (316.4–325.1)	5.9 (5.9–5.9)
6 w	65.3 (49.7–68.3)	226.4 (214.3–272.6)	211.5 (157.3–219.7)	5.9 (5.3–6.3)
8 w	108.1 (66.5–113.2)	215.5 (170–237)	208.2 (198.3–272.1)	5.5 (5.2–5.6)
10 w	82.3 (58.7–92.3)	191.2 (188.8–229.3)	384.3 (242.9–522.9)	5.4 (5.2–6)
12 w	76.35 (62.5–90.2)	212.15 (166.1–258.2)	190 (175.9–204.1)	5.6 (5.6–5.7)
	Carbon Tetrachloride Mice			
Control	137.1 (128.5–274)	989 (923.3–1054.7)	65.5 (54–79.3)	4.7 (4.6–5)
2 w	117.85 (117.7–118)	694.85 (666.2–723.5)	108.65 (93.9–123.4)	5.4 (4.7–6.1)
4 w	95.9 (78.8–113)	1070.55 (611.6–1529.5)	132.95 (131.5–134.4)*	5.25 (5–5.5)
6 w	174 (77.3–194.7)	1325.5 (599.9–1459)	121.8 (117–127.9)*	5.5 (5.3–6)
8 w	195.35 (163.2–227.5)	779.5 (538.8–1020.2)	110.95 (97.6–124.3)*	5.25 (5.2–5.3)
10 w	393.6 (322.1–594.8)	1430.3 (968.9–1791.2)	128.2 (118.8–134.5)*	5.6 (5–6.4)
12 w	100.1 (99.6–180)	512.2 (446.3–1276.7)	94 (93.3–105.4)*	4.6 (4.4–5)
	D–Galactosamine Rats			
Control	51.6 (48.7–61.5)	198.4 (178–220.2)	202 (154.3–268.9)	6.2 (6–6.3)
2 w	62.5 (53–66.9)	228.5 (172.6–245.6)	303.2 (245.2–340.6)	5.8 (5.7–6.1)
4 w	77.9 (67.8–87.4)*	220.3 (203.1–299.2)	276.7 (235–319.2)	6 (5.7–6.3)
6 w	59 (41.2–69.5)	211.6 (195.8–233.8)	343.3 (247.3–357.2)	5.9 (5.7–6)
8 w	60.8 (54.4–83.9)	194.6 (188.4–199.4)	283.7 (261.9–327.5)	5.6 (5.2–5.8)*
10 w	64.7 (58.8–73.4)	243.8 (193.2–262.5)	260.9 (195.8–335.8)	5.8 (5.5–5.9)*
12 w	58.2 (52.5–84.2)	253.5 (212.2–348.7)	333.5 (239.1–381.9)	6.1 (5.9–6.2)
	D–Galactosamine Mice			
Control	143.6 (134.6–206.8)	1049.6 (636–2328.7)	114.3 (105.6–119.6)	4.5 (4.4–5.1)
2 w	103.5 (76.5–183.9)	560.8 (453.1–1571.8)	125.3 (119–130)	4.7 (4.4–4.8)
4 w	195.2 (111.9–232)	1033.9 (279.7–1431)	121.8 (98.6–144.5)	5.1 (5–5.2)
6 w	155.05 (130–180.1)	1403 (780.5–2025.5)	117.25 (112.4–122.1)	5.3 (5.1–5.5)
8 w	124.4 (65.8–167.1)	626.8 (198.5–1672.2)	105.8 (86.1–107.2)	4.6 (4.5–5)
10 w	145 (92.6–153.5)	675.7 (504.8–1141.6)	105 (102.2–106)	4.7 (4.4–5)
12 w	94.1 (92.2–106)	605.3 (559.2–703)	98.7 (84.7–104.7)	4.5 (4.3–5)

Data are presented as median (min-max); n = 3. *$p < 0.05$, statistically significant as compared to controls.

liver parenchyma, including massive inflammatory infiltration around the central veins and hepatocyte necrosis, were observed at week 10 of intoxication (Fig. 1, Table 5).

In D-GalN-intoxicated rats, we observed mild hepatitis at weeks 4 and 6 of intoxication. During this period, we observed inflammatory infiltration in zone 1 of the hepatic acini (around portal areas) and ballooning degeneration around the central veins in zone 3. At a later time point, hepatitis slowly decreased (Fig. 1, Table 5).

We did not observe any histopathological changes in the livers of D-GalN-treated mice (Fig. 1, Table 5).

To sum up, in CCl_4 treated mice and rats the most advanced histopathological changes (irrespective of fibrosis evaluation) were visible from week 8 of intoxication. By contrast, in D-GalN models only minor histopathological changes were observed in rats and were not observed in mice.

3.3 Fibrosis Assessment

In animals of the control groups representing normal parenchymal architecture of the liver without fibrous expansion, the area of fiber deposition was 1% in rats and 0.37% in mice (Table 5, Figs. 2,3,4,5).

In the groups of CCl_4-treated rats, liver fibrosis began early, and after 2 weeks of intoxication it was observed in most pericentral areas of the livers. Between weeks 4 and 6, fiber morphology changed and the area of collagen deposition tended to increase. From week 6 of the experiment, we saw central-to-central bridging and fibrous expansion from most pericentral spaces. At this time, polarizing microscopy showed an increasing number of thick red and orange fibers. At week 12, formation of occasional cirrhotic nodules was observed (Table 5, Fig. 2).

In CCl_4-treated mice, from week 2 onwards we observed a fibrous expansion with occasional central-central

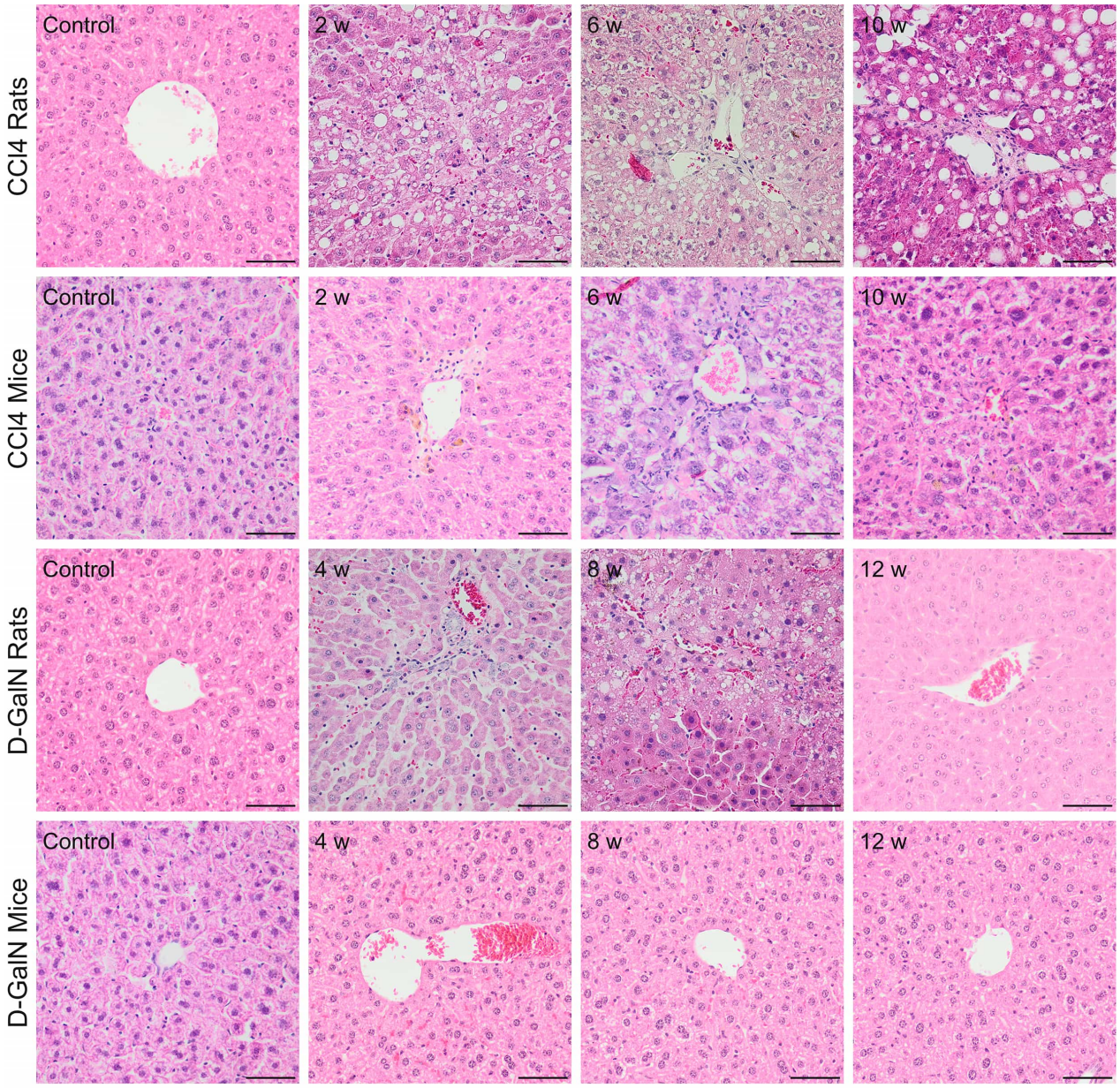

Fig. 1. Histopathological changes in zone 3 (pericentral) of the hepatic acinus in rats and mice after repeated CCl_4 or D-GalN injections. In CCl_4 treated rats, hepatocytes around the central veins containing lipid droplets were visible at weeks 4, 8, and 12 of intoxication. In mice, at 4 weeks after repeated CCl_4 injections, we observed minor ballooning degeneration around the central veins. In D-GalN-intoxicated rats, we observed mild inflammatory infiltrates around triads and central veins at week 4. At week 8 of intoxication, inflammatory infiltrates were visible along with ballooning degeneration. We did not observe any histopathological changes in the livers of D-GalN-treated mice. Mag. 200×, the scale bar represents 40 μm, H&E staining.

bridging in all pericentral areas and an increase in the total number of thick red and orange fibers. At week 6 of intoxication, we noted an increased number of red (thick) fibers in comparison to the control group ($p < 0.05$). At week 10 of intoxication, marked central-central bridging with dispersed fibers was developed, forming pericellular trabecular fibrosis with a "wire mesh" pattern. The ratio of red to orange fibers changed. At week 12, the total collagen fiber area ($p < 0.05$) and the number of thick red fibers increased significantly ($p < 0.05$) compared to control groups (Table 5, Fig. 3).

In D-GalN-treated rats, the first collagen depositions were observed at week 4. Polarizing microscopy showed fibrous expansion from some portal and pericentral areas and short septa corresponding to Ishak score 1 but no increased collagen area. After 8 weeks of intoxication, we noted moderate fibrosis with collagen deposition and an increasing number of thick red fibers (Table 5, Fig. 4).

In D-GalN-treated mice, minor liver fibrosis began at week 10. The semi-quantitative scale showed early fibrosis

Table 5. Histopathological assessment, including steatosis and fibrosis in the livers of rats and mice intoxicated with CCl_4 and D-GalN.

	Histopathological grading (0–4)		Steatosis (0–3)		Fibrosis: Ishak score (0–6)	
Carbon tetrachloride						
	Rats	Mice	Rats	Mice	Rats	Mice
Control	0	0	0	0	0	0
2 w	0	1	1	0	2	3
4 w	1	1	2	0	3	3
6 w	1	1	0	0	4	3
8 w	1	3	1	0	4	3
10 w	2	4	1	0	4	4
12 w	1	1	1	0	5	4
D-Galactosamine						
	Rats	Mice	Rats	Mice	Rats	Mice
Control	0	0	0	0	0	0
2 w	0	0	0	0	0	0
4 w	2	1	0	0	1	0
6 w	2	0	0	0	1	0
8 w	1	0	0	0	3	0
10 w	1	2	0	0	3	1
12 w	0	0	0	0	3	1

Histopathological grading is the median of three animals. n = 3.

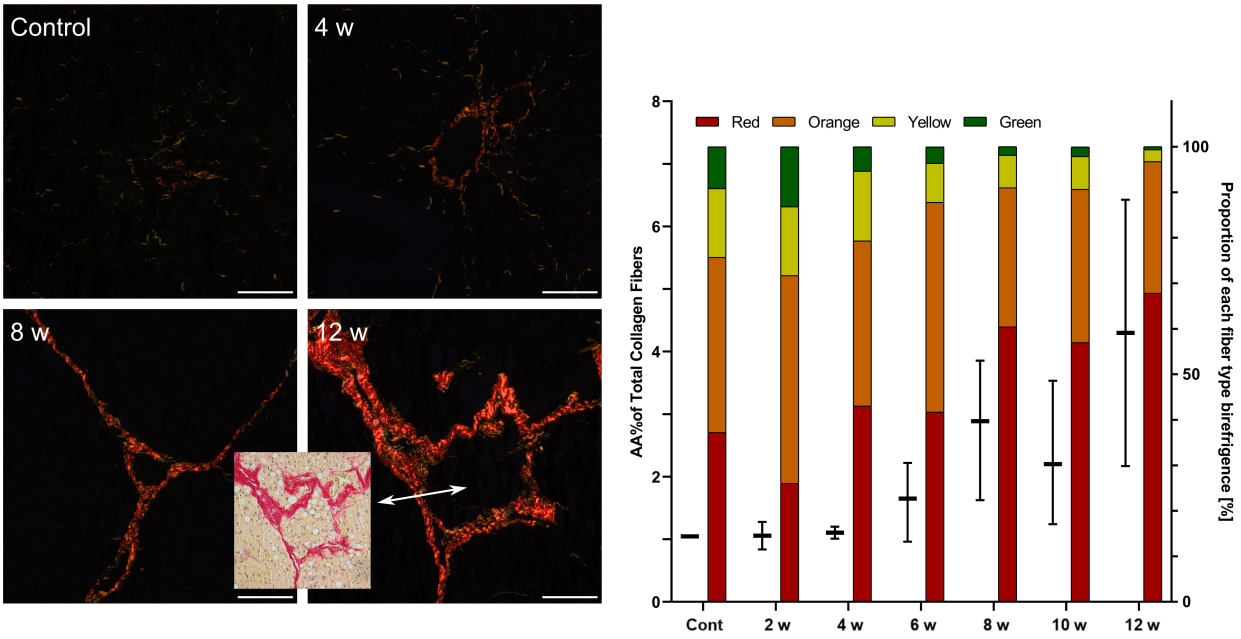

Fig. 2. Assessment of fibrosis in the livers of rats after repeated CCl_4 injections. Sirius red staining under polarized light. Mag. 200×; the scale bar represents 40 μm. The white arrow indicates cirrhotic nodules, which are also shown in Sirius red staining under visible light (middle picture, mag. 200×). The area fraction (%AA) occupied by collagen fibers is shown in a box-and-whiskers plot and %AA of individual fiber birefringence is shown in a bar chart (red, orange, yellow, and green), which indicates decreasing thickness of the fibers. Data are presented as median (min-max).

without a significant increase in collagen deposition at any time point (Table 5, Fig. 5).

The onset of the different stages of liver fibrosis in the studied models is presented in Table 6. At week 12 of CCl_4 intoxication, one rat showed regenerative nodules. Literature data indicate progression of incomplete cirrhosis at this time point [11].

To summarize the stages of liver fibrosis in both experimental models, we found that in CCl_4 intoxicated rodents early fibrosis was observed as early as after 2 weeks of experiment, and established fibrosis was visible from week 6 of experiment. Among all tested models, incomplete cir-

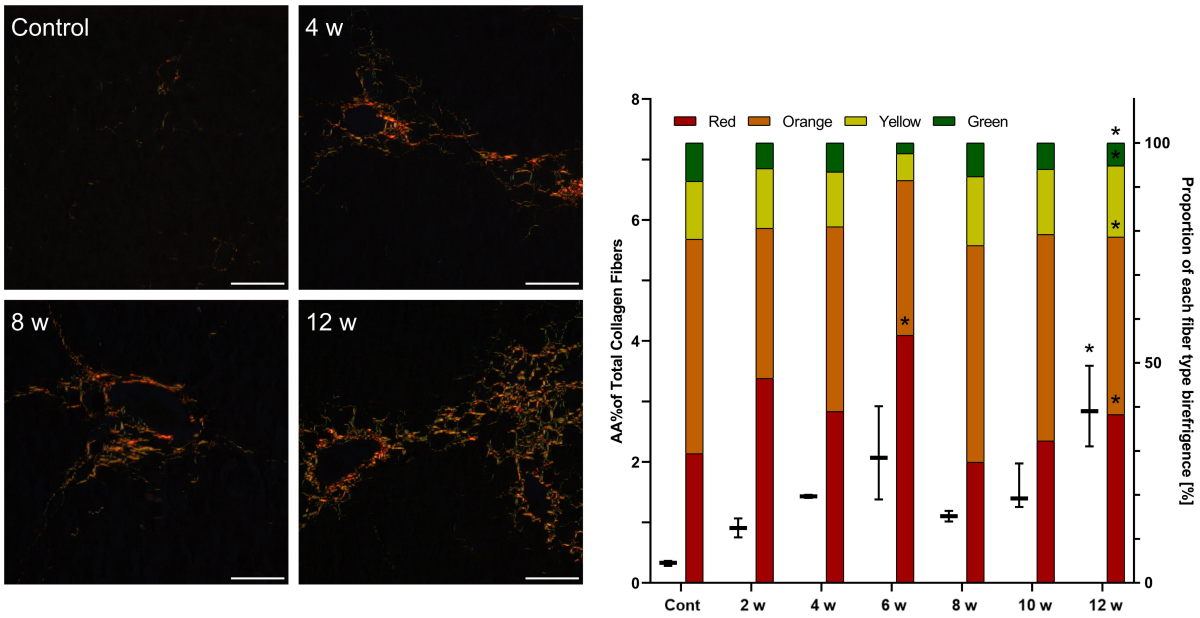

Fig. 3. Assessment of fibrosis in the livers of mice after repeated CCl_4 injections. Sirius red staining under polarized light. Mag. 200×; the scale bar represents 40 μm. The %AA occupied by collagen fibers is shown in a box-and-whiskers plot and %AA of individual fiber birefringence is shown in a bar chart (red, orange, yellow, and green), which indicates decreasing thickness of the fibers. *$p < 0.05$ as compared to the control. Data are presented as median (min-max).

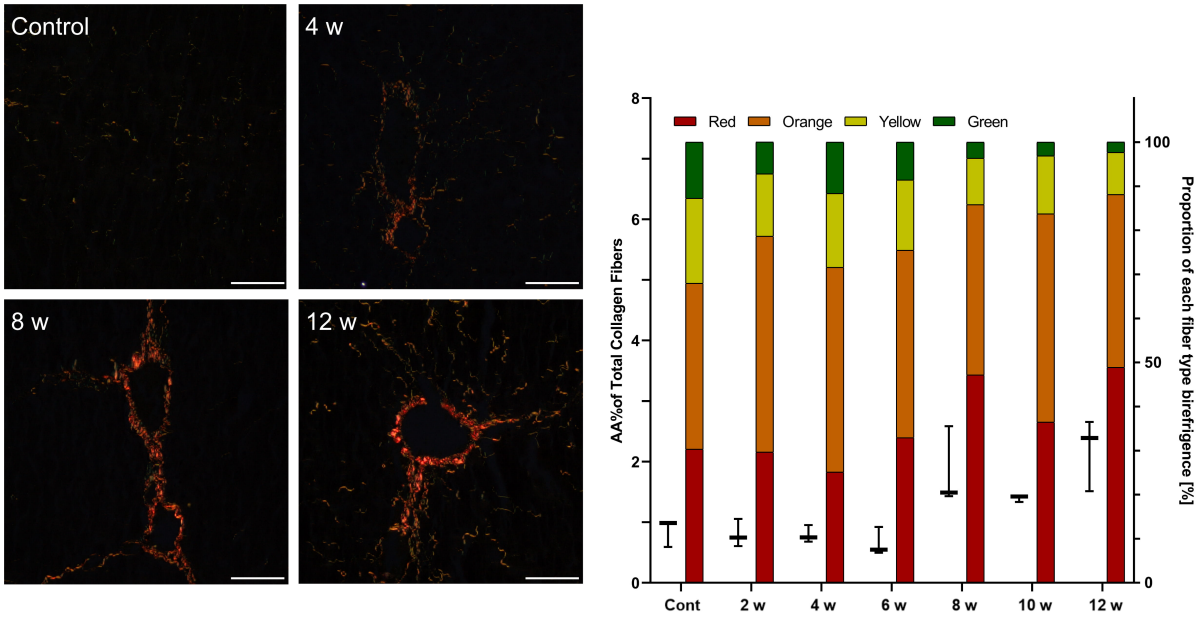

Fig. 4. Assessment of fibrosis in the livers of rats after repeated D-GalN injections. Sirius red staining under polarized light. Mag. 200×; the scale bar represents 40 μm. The %AA occupied by collagen fibers is shown in a box-and-whiskers plot and %AA of individual fiber birefringence is shown in a bar chart (red, orange, yellow, and green), which indicates decreasing thickness of the fibers. Data are presented as median (min-max).

rhosis were noted only in rats after 12 weeks of CCl_4 intoxication (Table 6). In D-GalN models, first sign of liver fibrosis in rats (week 4) and mice (week 10) were visible later as compared to appropriate CCl_4 treated groups, and fibrosis was late (week 8 in rats) or not observed (in mice) (Table 6).

3.4 Hepatic Stellate Cells Activation

After repeated CCl_4 injections to rats, we observed minor (2- to 4-fold) increase in the area occupied by α-SMA$^+$ cells at weeks 2, 4, and 6 compared to the control group ($p < 0.05$). In CCl_4-intoxicated mice, the area occupied by α-SMA$^+$ cells was increased in some groups (sig-

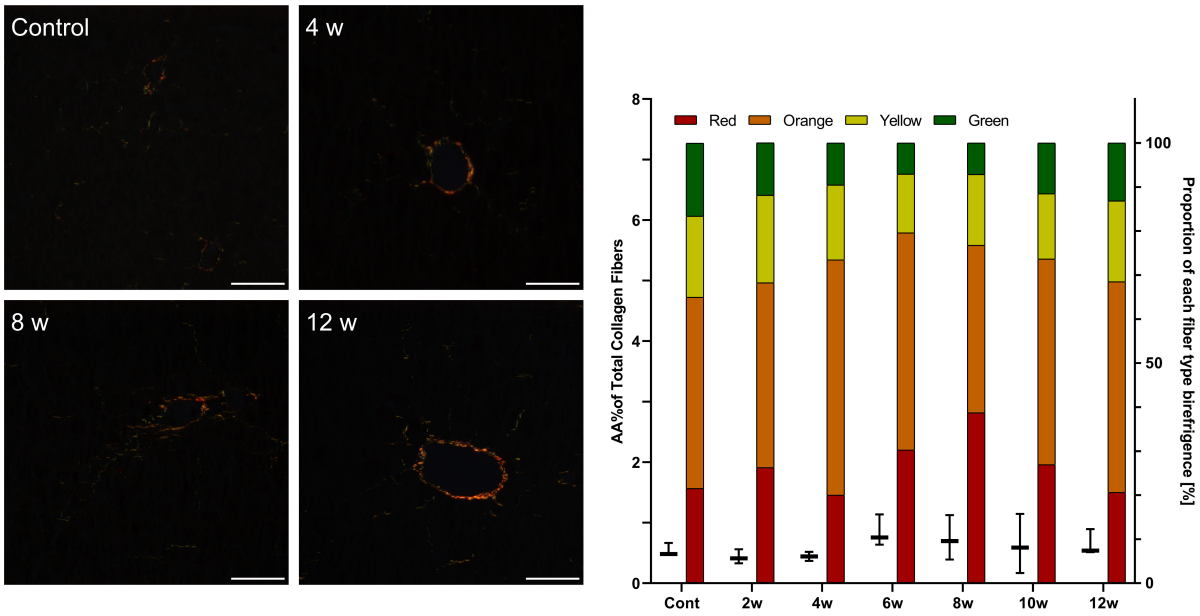

Fig. 5. Assessment of fibrosis in the livers of mice after repeated D-GalN injections. Sirius red staining under polarized light. Mag. 200×; the scale bar represents 40 μm. The %AA occupied by collagen fibers is shown in a box-and-whiskers plot and %AA of individual fiber birefringence is shown in a bar chart (red, orange, yellow, and green), which indicates decreasing thickness of the fibers. Data are presented as median (min-max).

Table 6. Stages of liver fibrosis in experimental models.

	First sign of liver fibrosis	Early fibrosis	Established fibrosis	Incomplete cirrhosis
CCl_4 rats	-	2nd week	6th week	12th week
CCl_4 mice	-	2nd week	6th week	-
GalN rats	4th week	8th week	-	-
GalN mice	10th week	-	-	-

The criteria for each stage of liver fibrosis were as follow: first sign of liver fibrosis (Ishak score 0–1 and no increased in the area of collagen fibers); early fibrosis (Ishak score 2–3 or increased in the area of collagen fibers); established fibrosis (Ishak score 4 and increased in the area of collagen fibers); and incomplete cirrhosis (Ishak score 5 and increased in the area of collagen fibers).

nificantly at week 8 ($p < 0.05$)) compared to the control group. In rats and mice repeatedly injected with D-GalN, we did not observe an increase in the area occupied by α-SMA$^+$ cells Fig. 6.

The results indicated the stronger hepatic stellate cells activation in CCl_4 experimental models than in D-GalN models confirming greater fibrogenic potential of CCl_4–treated rat and mouse livers.

3.5 Proliferative and Apoptotic Activities

Rats repeatedly injected with CCl_4 presented an elevated ($p < 0.05$) number of Ki-67$^+$ cells at weeks 2 and 10, and mice at week 2, 4, 8, and 10 week ($p < 0.05$). Rats treated with D-GalN showed slightly elevated proliferation in most groups (statistically significant at week 4 ($p < 0.05$)). Mice treated with D-GalN presented an increased ($p < 0.05$) number of Ki-67$^+$ cells at weeks 4 and 6 week of intoxication (Fig. 7).

Minimal and moderate numbers of Cas3$^+$ cells were observed in CCl_4-treated rats up to week 6. After this time, we did not observe any signs or symptoms of apoptosis. In CCl_4-treated mice, Cas3 expression was observed at all time points, peaking at weeks 8 and 10. In D-GalN treated rats, moderate numbers of Cas3$^+$ cells were observed at weeks 4 and 6 of intoxication. No significant apoptotic activity was observed in D-GalN-treated mice Fig. 8.

The results indicated the coincidence of changes in apoptotic and proliferative activities in livers, especially of CCl_4-treated mice, indicating the simultaneous action of injury and repair processes. The pattern of fluctuations in proliferative and apoptotic activity observed in rats and mice chronically treated with D-GalN indicated low potential of D-GalN to induce apoptosis in mice.

3.6 Gene Expression Related to Chronic Liver Injury

We observed very low expression of *Gadd45a*, *COL1A1*, *IL-6*, and *TNF*α in mouse and rat liver samples (data not shown).

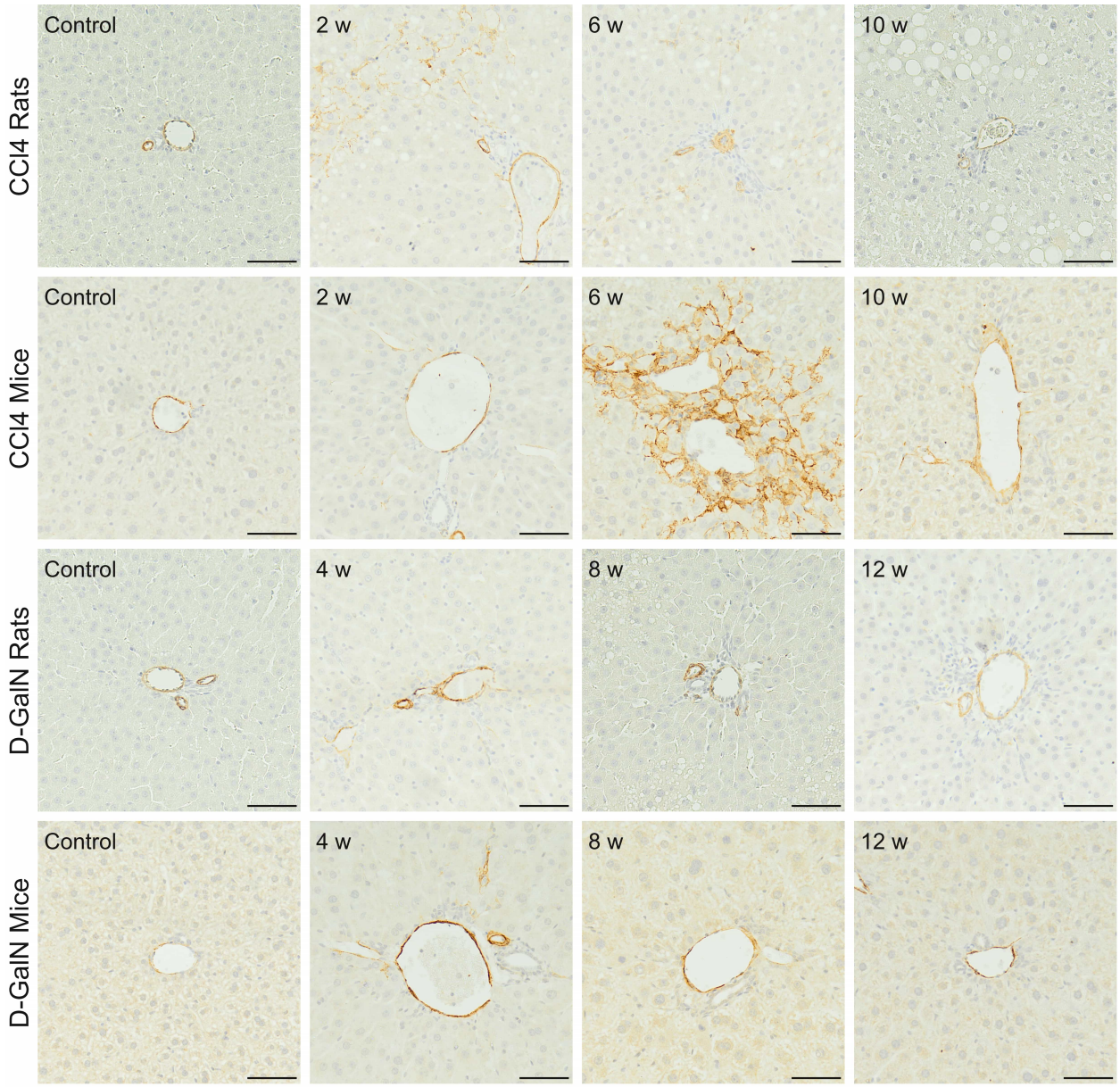

	Control	2 w	4 w	6 w	8 w	10 w	12 w
CCl4 Rats	0.01 (0.00-0.01)	0.11 (0.10-0.12)*	0.25 (0.02-0.48)*	0.13 (0.10-0.25)*	0.25 (0.01-0.43)	0.07 (0.01-0.08)	0.08 (0.01-0.14)
CCl4 Mice	0.04 (0.01-0.11)	0.35 (0.01-0.69)	0.12 (0.03-0.21)	0.01 (0.01-0.06)	0.65 (0.62-0.67)*	0.07 (0.01-0.78)	0.11 (0.03-0.14)
D-GalN Rats	0.02 (0.01-0.32)	0.04 (0.01-0.18)	0.08 (0.01-0.23)	0.21 (0.04-0.45)	0.02 (0.01-0.38)	0.06 (0.01-0.15)	0.06 (0.01-0.13)
D-GalN Mice	0.12 (0.01-0.3)	0.05 (0.01-0.26)	0.3 (0.01-0.42)	0.04 (0.01-0.08)	0.24 (0.12-0.71)	0.13 (0.01-0.96)	0.04 (0.01-0.12)

Fig. 6. Immunodetection of α-SMA$^+$ cells in the vascular wall (smooth muscle cells) and Disse spaces (stellate cells) in the livers of rats and mice treated with CCl_4 and D-GalN. Microphotographs show zone 1 of the hepatic acinus. Mag. 200×; the scale bar represents 40 μm. Expression of α-SMA in stellate cells is summarized in the table below as medians of positively stained cells per field (0.3779 mm^2) (min-max); n = 3. *$p < 0.05$ as compared to the control.

Gene expression of *COL3A1* in CCl_4-treated rats was stable and the observed changes were not statistically significant. In mice intoxicated with CCl_4, we observed significant (3- to 9-fold) increase in *COL3A1* gene expression between weeks 2 and 12 ($p < 0.05$) of the experiment compared to the control group. In the D-GalN-treated groups, there were a statistically significant increases in *COL3A1* mRNA expression at weeks 4 and 6 in rats and between

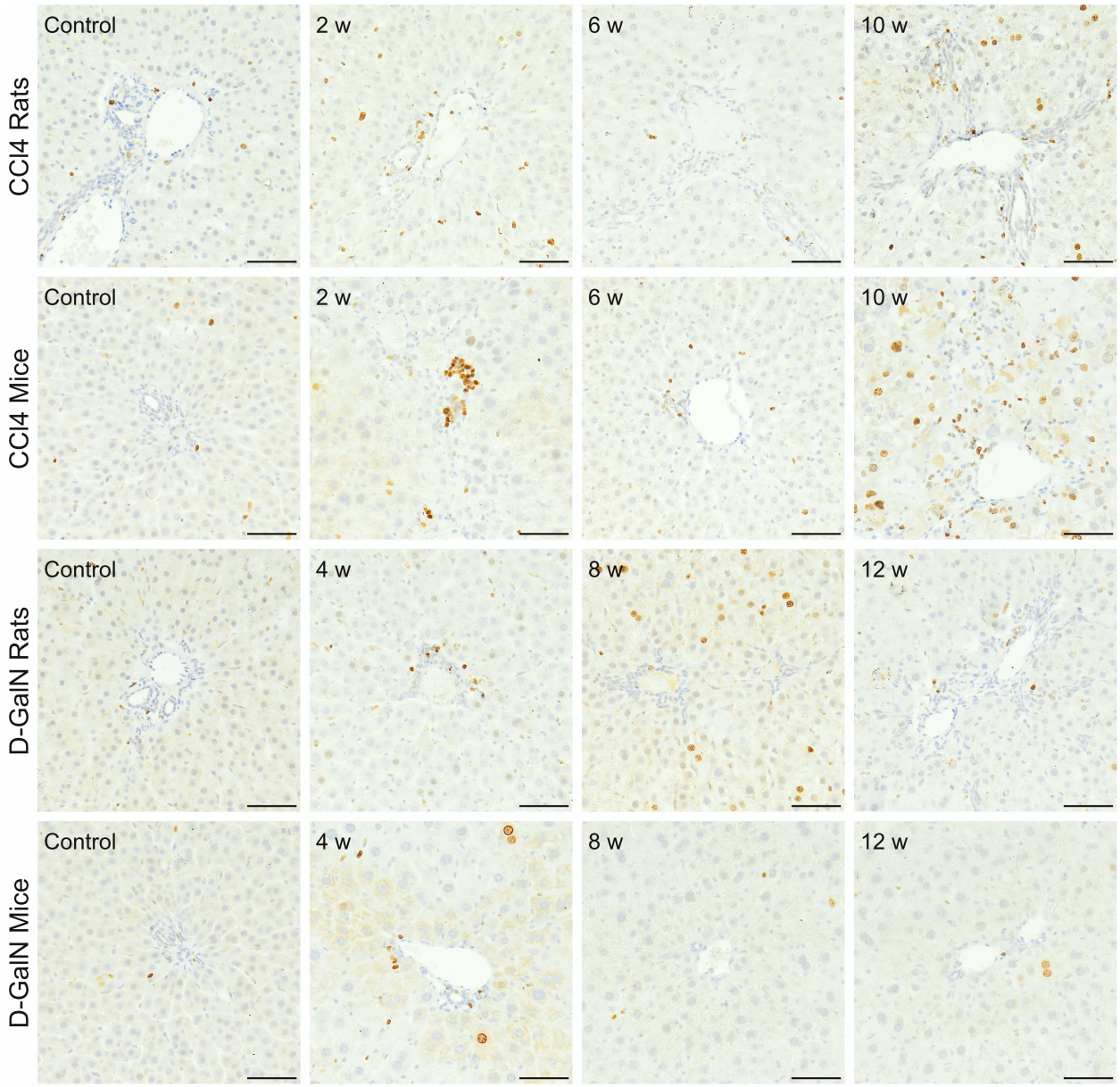

	Control	2 w	4 w	6 w	8 w	10 w	12 w
CCl4 Rats	43.5 (22.8-48.8)	116.6 (79.0-154.2)*	58.7 (49.6-67.7)	30.8 (19.6-33.3)	35.1 (29.3-67.3)	197.2 (112.1-217.8)*	111.0 (65.3-156.7)
CCl4 Mice	43.8 (9.4-45.0)	103.5 (100.8-106.2)*	68.6 (61.0-76.3)*	40.6 (35.1-41.5)	117.9 (101.0-134.8)*	286.6 (261.2-369.2)*	61.6 (48.3-66.8)
D-GalN Rats	35.9 (21.3-65.1)	68.4 (25.2-87.2)	57.8 (50.8-159.6)*	45.2 (35.5-252.0)	141.9 (75.5-192.2)	60.8 (23.7-62.1)	42.4 (28.3-62.3)
D-GalN Mice	23.0 (21.6-28.1)	28.6 (24.4-46.1)	166.2 (150.3-187.8)*	64.4 (30.6-203.0)*	27.3 (16.6-97.8)	31.5 (15.3-47.3)	40.5 (22.7-45.9)

Fig. 7. Immunodetection of Ki67$^+$ cells in the livers of rats and mice treated with CCl_4 and D-GalN. Microphotographs show zone 1 of the hepatic acinus. Mag. 200×; the scale bar represents 40 μm. Cell proliferation is summarized in the table below as medians of Ki67$^+$ cells per field (0.3779 mm^2) (min-max); n = 3. *$p < 0.05$ as compared to the control.

weeks 2 and 8 in mice compared to the control groups (Table 7).

In CCl_4-treated rats and mice, we noted a significantly decreased *CYP2E1* expression at most time points and a 2- to 3-fold lower expression at weeks 4, 8, and 10, respectively, compared to the control group.

We observed an increase in *CYP2E1* gene expression in rats between weeks 4 and 12 and a temporary increase in mice at weeks 2 and 4, both treated with D-GalN. In rats, it was statistically significant at weeks 4, 6, and 12 ($p < 0.05$).

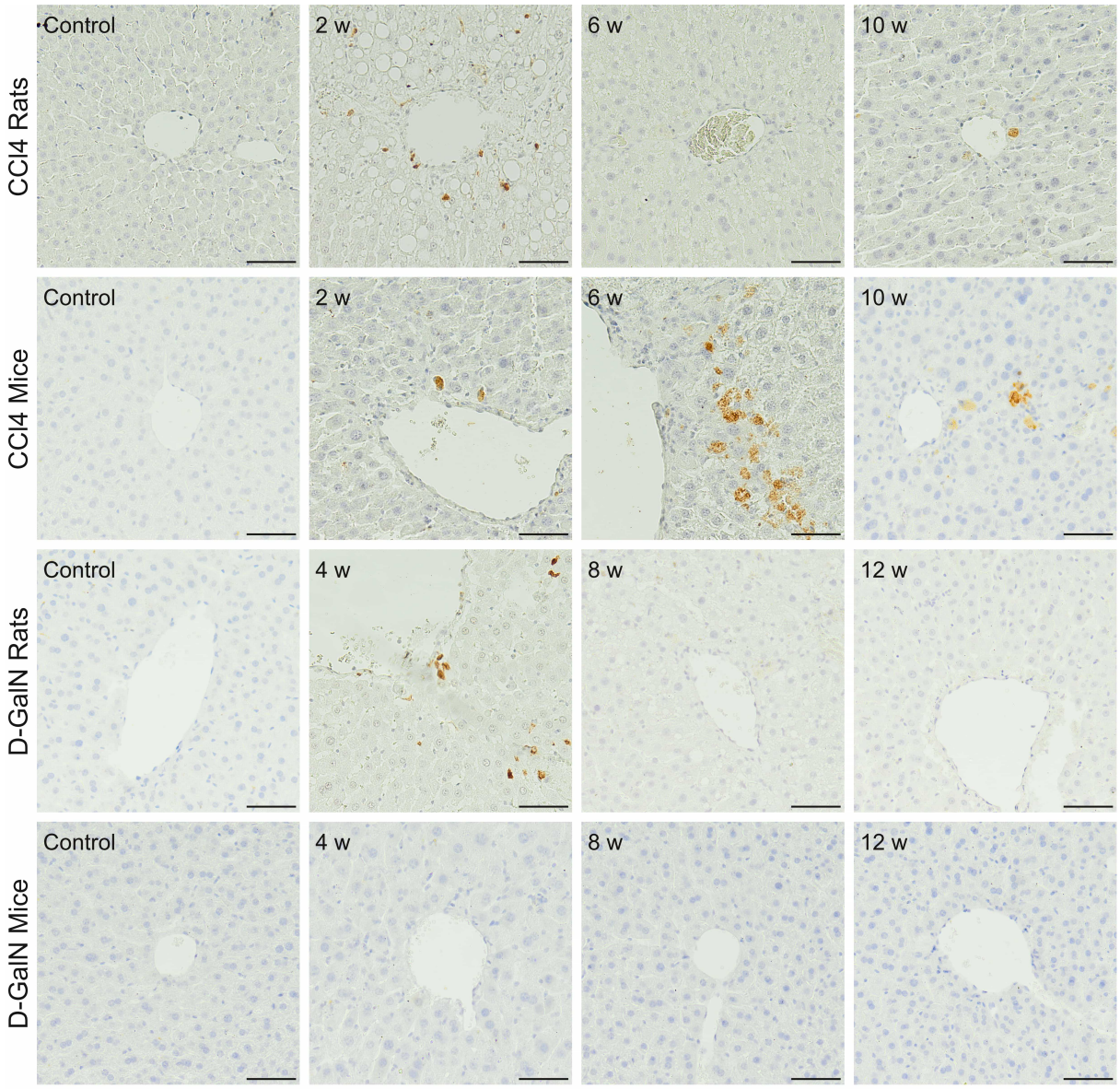

	Control	2 w	4 w	6 w	8 w	10 w	12 w
CCl4 Rats	0	1	2	2	0	0	1
CCl4 Mice	0	2	1	2	3	4	2
D-GalN Rats	0	0	2	2	0	0	0
D-GalN Mice	0	0	0	0	0	0	0

Fig. 8. Immunodetection of Cas-3$^+$ cells in the livers of rats and mice treated with CCl_4 and D-GalN. Microphotographs show the liver parenchyma around the central veins (zone 3 of the hepatic acinus). Mag. 200×; the scale bar represents 40 μm. The semi-quantitative scale of cleaved caspase-3 immunoreactivity was as follows: (0) no positive cells; (1) few (<10) positive cells per field; (2) 10–25 positive cells per field; (3) 25–50 positive cells per field; (4) >50 positive cells per field and/or clusters of apoptotic cells. The presented data are the median values of three animals.

In mice, this was followed by a downward trend at weeks 8 ($p < 0.05$) and 10.

There were noticeable but (at most time points) not statistically significant differences in *PPARα* mRNA expression between control and CCl_4-treated rats and mice. These changes were characterized by alternate increases and decreases during the 12-week observation period.

In D-GalN-intoxicated rats, we observed a significantly increased *PPARα* expression at week 6 followed by its a decreased expression at week 10 compared to the control group. There was also significant decrease in *PPARα* expression in D-GalN-intoxicated mice over the same period ($p < 0.05$).

In CCl_4-treated rats and mice, we observed a significant decrease in *cMet* expression only at week 12 in the

Table 7. Expression of the genes *COL3A1*, *CYP2E1*, *PPARα*, *c-Met*, and *HGF* in the livers of rats and mice intoxicated with CCl_4 and D-GalN.

Time point	COL3A1	CYP2E1	PPAR	c-Met	HGF
	Carbon Tetrachloride Rats				
Control	0.103 (0.067–0.263)	1.974 (1.381–3.826)	0.178 (0.081–0.231)	0.079 (0.013–0.132)	0.048 (0.038–0.100)
2 w	0.180 (0.121–0.233)	1.069 (0.782–2.372)*	0.125 (0.104–0.152)	0.103 (0.007–0.155)	0.021 (0.016–0.026)*
4 w	0.028 (0.013–0.242)	2.021 (1.564–2.151)	0.376 (0.143–0.690)	0.051 (0.015–0.094)	0.036 (0.011–0.052)
6 w	0.120 (0.018–0.327)	0.657 (0.255–1.590)*	0.103 (0.032–0.143)	0.039 (0.020–0.128)	0.063 (0.029–0.510)
8 w	0.115 (0.097–0.184)	0.967 (0.508–1.743)*	0.097 (0.067–0.222)	0.066 (0.063–0.083)	0.069 (0.037–0.128)
10 w	0.137 (0.050–0.234)	1.454 (0.663–2.261)*	0.314 (0.069–0.513)	0.053 (0.012–0.066)	0.050 (0.026–0.110)
12 w	0.146 (0.074–0.171)	2.255 (0.744–3.846)	0.276 (0.077–0.29)	0.019 (0.005–0.037)*	0.035 (0.011–0.043)*
	Carbon Tetrachloride Mice				
Control	0.046 (0.031–0.062)	28.052 (19.226–34.896)	0.771 (0.189–1.106)	0.156 (0.106–0.309)	0.070 (0.048–0.152)
2 w	0.397 (0.179–0.485)*	32.391 (15.313–39.854)	0.611 (0.397–0.691)	0.133 (0.095–0.189)	0.161 (0.054–0.255)
4 w	0.251 (0.172–0.312)*	15.665 (10.438–52.482)*	0.387 (0.233–0.743)	0.049 (0.014–0.117)*	0.223 (0.137–0.290)*
6 w	0.145 (0.133–0.231)*	26.709 (26.067–35.119)	0.660 (0.446–1.16)	0.099 (0.090–0.155)	0.092 (0.078–0.127)
8 w	0.300 (0.244–0.309)*	8.253 (6.737–36.560)	0.285 (0.126–0.883)	0.266 (0.192–0.340)	0.019 (0.016–0.021)*
10 w	0.388 (0.327–0.420)*	9.302 (5.936–12.812)*	0.149 (0.125–0.208)*	0.097 (0.061–0.133)	0.166 (0.071–0.268)
12 w	0.161 (0.114–0.236)*	48.001 (37.923–70.767)*	1.035 (0.671–2.723)	0.097 (0.023–0.223)*	0.077 (0.023–0.132)
	D–Galactosamine Rats				
Control	0.091 (0.06–0.161)	4.766 (1.331–6.203)	0.501 (0.308–0.617)	0.061 (0.032–0.079)	0.183 (0.062–0.242)
2 w	0.096 (0.062–0.124)	3.382 (3.108–3.962)	0.290 (0.262–0.459)	0.029 (0.017–0.043)*	0.093 (0.045–0.15)
4 w	0.226 (0.143–0.346)*	8.344 (6.684–14.527)*	0.600 (0.415–1.320)	0.028 (0.014–0.212)	0.160 (0.127–0.483)
6 w	0.250 (0.052–0.361)*	12.197 (10.618–28.413)*	1.751 (0.840–2.054)*	0.059 (0.017–0.140)	0.092 (0.066–0.341)
8 w	0.056 (0.025–0.089)*	6.326 (3.227–8.282)	0.255 (0.143–0.287)*	0.036 (0.023–0.042)*	0.052 (0.027–0.106)*
10 w	0.063 (0.030–0.088)*	7.122 (1.03–16.248)	0.369 (0.056–0.698)	0.029 (0.016–0.059)*	0.093 (0.088–0.098)*
12 w	0.070 (0.030–0.107)	6.928 (5.867–10.074)*	0.522 (0.326–0.652)	0.028 (0.014–0.044)	0.152 (0.078–0.276)
	D–Galactosamine Mice				
Control	0.052 (0.023–0.082)	34.028 (13.817–55.267)	1.041 (0.682–1.432)	0.258 (0.067–0.373)	0.167 (0.009–0.187)
2 w	0.107 (0.059–0.229)*	77.442 (57.083–102.893)*	0.495 (0.066–1.306)	0.263 (0.143–0.319)	0.179 (0.067–0.185)
4 w	0.096 (0.077–0.209)*	89.884 (33.121–127.972)*	0.757 (0.253–1.264)	0.236 (0.126–0.338)	0.032 (0.015–0.054)
6 w	0.127 (0.049–0.199)*	58.541 (40.530–172.545)	0.319 (0.295–1.671)	0.115 (0.048–0.406)	0.098 (0.032–0.255)
8 w	0.087 (0.033–0.105)*	15.291 (12.719–26.518)	0.994 (0.181–0.992)	0.040 (0.038–0.060)*	0.013 (0.002–0.160)*
10 w	0.035 (0.031–0.038)	18.319 (12.084–26.264)	0.235 (0.132–0.462)*	0.080 (0.073–0.098)*	0.024 (0.003–0.057)*
12 w	0.062 (0.053–0.110)	41.135 (30.376–47.368)	0.673 (0.523–0.740)	0.108 (0.093–0.248)	0.117 (0.092–0.368)

Data are presented as a median of $2^{-\Delta Ct}$ (min-max); n = 3. *$p < 0.05$, statistically significant as compared to controls.

case of rats and at weeks 4 and 12 in the case of mice. A similar trend was noticed in D-Gal-treated rats (at weeks 2, 8, and 10) and D-Gal-treated mice (at weeks 8 and 10).

We observed small but statistically significant decreases in *HGF* gene expression in rats treated for 2 and 12 weeks with CCl_4. Mice treated with CCl_4 showed more significant fluctuations, characterized by an increase in expression at weeks 2 and 4, followed by a decrease at weeks 6 and 8, and a renewed increase after week 10.

In D-GalN-treated rats and mice, we observed a decrease in *HGF* expression after weeks 6 and 4, respectively, followed by a return to control values at week 12.

4. Discussion

In this study, we assessed the progression of histopathological changes in the livers of experimental animals, in the chronic liver injury model, to select the best time for potential pharmaceutical or stem cell therapy. During long-term intoxication, in response to parenchymal inflammatory reaction, stellate cells produce collagen and other extracellular matrix components. Collagen fibers enter the perisinusoidal space of Disse and, as it were, seal the permeable barrier between the sinusoids and the liver parenchyma, effectively inhibiting the flow of substances and migration of administered cells that could leave the vascular bed. It has been observed that in people without liver fibrosis, this organ is a frequent site of metastasis of malignant tumors from other organs due to the favorable hemodynamic conditions of flowing blood, permeability of the sinusoidal wall, and the small diameter of sinusoids, which favors the formation of microemboli from circulating cells. The resulting emboli retain cells within the vascular net-

work of the organ, promoting their migration into the liver parenchyma, which would be impossible if the cells were suspended in the flowing bloodstream [38]. In contrast, metastases from distant organs are found very rarely in patients with developed cirrhosis.

Nevertheless, cirrhosis itself requires treatment which, in addition to eliminating etiological factors, involves slowing down the progression of the disease, including fibrosis, and supporting the functioning of the liver. Failures of CLD cell therapies were most likely due to unfavorable biodistribution of the administered cells caused by advanced fibrosis [39,40]. So far, no detailed model studies have been conducted to analyze how the duration of the intoxication, and thus the degree of fibrosis, affects the biodistribution of stem cells administered for therapeutic purposes [11,14,41–44].

Experimental models used to induce liver injury include intoxication with CCl_4 or D-GalN. The main mechanism of liver injury by CCl_4 involves its cytochrome P450 (CYP)-dependent biotransformation resulting in free radical generation, cell membrane oxidation, cytoplasmic ion imbalance, DNA damage, necrotic cell death, and inflammation [45]. In the groups where mice and rats were intoxicated with repeated injections of CCl_4, we observed a decrease in CYP2E1 expression at some time points, which may be related to advanced histopathological changes and secondary hepatocyte damage via a free radical mechanism, and is consistent with the observations that CCl_4 is a potent CYP2E1 inhibitor [46,47]. On the other hand, the slight increase in CYP2E1 expression observed by us in mice and rats intoxicated with D-GalN at certain time points literature data confirmed a small effect of D-GalN-intoxication on CYP2E1 expression in rodents [48–50].

D-GalN is a highly hepatospecific compound. Unlike other hepatotoxins, D-GalN does not directly damage other organs and does not cause irritation when injected. In hepatocytes, D-GalN is eliminated by the galactose metabolic pathway, including D-GalN phosphorylation to galactosamine-1-phosphate (GalN-1-P), followed by its conversion to UDP-galactosamine, which has a higher affinity for uridine diphosphate (UDP) than for galactose. The trapping effect leads to uridine deficiency, inhibition of RNA and protein synthesis, and apoptotic cell death [51].

The primary lasting effect of our intoxication procedures was the progressive liver fibrosis. The mechanism of fibrosis in models using CCl_4 and D-GalN is based on an inflammatory reaction initiated by damage to the liver parenchyma. In response to inflammation, hepatocytes and Kupffer cells produce, among others, TGF-β and PDGF, which are involved in the activation of stellate cells responsible for the process of synthesize extracellular matrix components and fibrosis through the deposition of a large amount of collagen I and moderate amounts of collagens III and IV in the perisinusoidal space [44,52,53]. We found that the groups of CCl_4-intoxicated rats and mice, where the dynamics of fibrosis were fastest, had the greatest increase in the percentage area occupied by α-SMA$^+$ stellate cells.

The data obtained by us and other research teams suggest that the onset of fibrosis in the models using CCl_4 occurs very early [3,37,38], and the rapid dynamics of its progression make it possible to distinguish different stages of organ fibrosis. In rats and mice chronically intoxicated with CCl_4, we observed early fibrosis in the form of fibrous expansion of collagen fibers from some pericentral areas at week 2 of intoxication. Both groups developed established fibrosis after 6 weeks of CCl_4 intoxication. In other studies, both in mouse and rat models using CCl_4, the development of established fibrosis was also observed between weeks 8 and 12 of intoxication [54–57]. Bubnov *et al*. [12], who used the same dose and regimen of intoxication as in our experiment, based on ultrasound examination and standard staining of liver sections, suggest the development of cirrhosis in rats at week 8 of intoxication. Nevertheless, in rats at week 12 we observed the presence of regenerative nodules indicative of the development of incomplete cirrhosis. Overall, the data we obtained, in particular the morphometric analysis of the percentage area occupied by collagen fibers in the liver parenchyma and the Ishak score, suggest the onset of early cirrhosis in rats as late as at week 12 of intoxication. Studies in C57B mice using the same xenobiotic dose and intoxication regime as in our study (12.5 μL/100 g CCl_4 bw every fifth day) showed the development of established fibrosis after 4 weeks and of incomplete cirrhosis after 8 weeks [11], indicating that the BALB/c mouse strain is less prone to develop fibrosis than the C57B strain [58]. In order to obtain a picture of cirrhosis produced in mice, it would be necessary to extend the duration of intoxication with CCl_4, e.g., to 20 weeks and/or to increase its dose, e.g., to 30 μL/100 g [59]. In CCl_4-intoxicated rats, where fibrosis was most evident, we noted an upward trend in the percentage of thick collagen fibers with a simultaneous decrease in the percentage of thin fibers over time. The process of pathological fibrosis is accompanied by an extracellular growth of collagen fibers in thickness. Our observation is consistent with literature data suggesting a relationship between an increase in the percentage of larger-diameter fibers and the processes of pathological fibrosis, aging of the body, and would healing [23,48,49].

At the molecular level, the process of fibrosis is influenced by a number of factors, and in particular depends on the expression of the genes *TGFβ*, *COL1A1*, and *COL3A1*. Increased expression of these genes results in the deposition of collagen at necrotic sites and formation of connective tissue scars. Increased amounts of type III collagen are found in many fibrotic conditions, such as liver and kidney fibrosis. However, these parameters are not used in routine clinical practice during the diagnosis and assessment of prognosis of CLD as their expression level does not correlate with the severity of the disease [60]. Transforming

growth factor-β (TGFβ) is an inflammatory cytokine that stimulates stellate cells to produce collagen and plays an important role during the development of chronic liver injury in both experimental animals and humans [14]. TGF-β promotes fibrogenesis in three different ways: it inhibits extracellular matrix degradation by inhibiting matrix metalloproteinases; it induces myofibroblast formation; and it induces matrix production through SMAD protein-dependent or -independent mechanisms [61]. In general, animal experiments indicate that the expression of genes responsible for fibrosis fluctuates over time [62]. As a result, despite the intensification of the extracellular processes of thickening of collagen fibers seen in microscopic images, we found a very low expression of the *COL1A1* gene in the test animals, stable expression of COL3A1 in rats, and increased expression of *COL3A1* in CCl_4-intoxicated mice (at all studied time points).

We observed morphological features of liver injury accompanying the fibrosis resulted from chronic liver injury [12], where the CCl_4 dose in intoxicated rats was gradually reduced during the experiment. These changes were such as ballooning degeneration, inflammatory infiltration, hepatocyte edema, signs of organ steatosis in the form of lipid droplets in the cytoplasm of hepatocytes, and necrosis, mainly within zone 3 of the hepatic acinus, i.e., around the central vein. In mice intoxicated with repeated injections of 12.5 μL/100g bw CCl_4, we observed the same features and localization of liver injury as in rats. However, in mice we did not observe liver steatosis. Thus, histopathological changes in mice and rats were localized similarly to those in chronic viral hepatitis or alcohol-induced liver fibrosis [63].

An additional effect of liver injury in the CCl_4 models was an increase in proliferative activity and/or in apoptotic activity of hepatocytes in rats and in mice. The coincidence of changes in apoptotic and proliferative activities in these models may indicate the simultaneous action of injury and repair processes of variable intensity associated with alternating injury and restoration of the structure and function of the liver [64]. Similar dynamics of injury also occur in humans in viral hepatitis and chronic alcohol consumption, where damage progresses during disease exacerbations, while during remissions, functional and morphological regeneration of the organ occurs [65]. It was shown in acute liver diseases that increased expression of HGF and its receptor c-Met induces hepatocyte proliferation and organ regeneration. Decreased HGF expression in chronic diseases is explained by a partial loss of the ability of the liver parenchyma to regenerate [41,66].

In the liver fibrosis models using repeated injections of D-GalN (25 mg/100 g bw in rats and 75 mg/100 g in mice), we observed the slow dynamics of fibrosis progression over time. Microscopic changes were accompanied by a transient increase in *COL3A1* gene expression. Similar changes, especially in mice, have been previously noted by other researchers. In the rat models using repeated injections of 25 mg/100 g D-GalN bw, the presence of early or established fibrosis was demonstrated at week 12 of intoxication [14,62]. In order to induce irreversible cirrhosis in the rat model, the duration of the intoxication should be extended to up to 6 months [67]. In the mouse model, an attempt to induce cirrhosis with a relatively high dose of 150 mg/100 g D-GalN bw administered regularly once a week for 13 weeks failed [68]. Overall, our results and literature data suggest that the rat and mouse models of CLD using repeated D-GalN injections offer significantly less opportunity to achieve established liver fibrosis and cirrhosis within a predictable and defined period of frame.

Fibrosis observed in D-GalN-intoxicated rats was accompanied by a relatively small inflammatory reaction and weakly pronounced visible histopathological changes, such as hepatocyte edema and ballooning degeneration. In the mouse model of chronic D-GalN administration, we did not observe any significant histopathological changes. In both rat and mouse models of D-GalN-induced CLD, other researchers observed little or no damage to the liver parenchyma [14]. Also, the increase in apoptotic activity only at certain time points after intoxication in rats, lack of apoptotic activity in mice, and temporary tendency to increase in proliferative activity observed in both rats and mice indicate relatively low potential of the D-GalN doses administered chronically to induce CLD. The scant literature data indicate a small effect of repeated low-dose injections of D-GalN on the induction of apoptosis [14,62]. Increased apoptotic activity in the liver parenchyma is much more pronounced in the acute or fulminant injury model, where a single injection of high doses of D-GalN is used [69,70]. Nevertheless, the decrease in the expression of the *HGF* gene and its receptor c-Met, found in animal groups studied by us, mostly those treated with D-GalN, coincides partially with literature data, which describe an increase in HGF expression in the initial stage of chronic hepatitis and a decrease in the expression of this gene in the advanced stage of the disease [66].

It should be noted that the histopathological changes recorded in the rat and moue livers in both intoxication models were not clearly reflected in the results of tests carried out on the blood of the test animals. In the models using CCl_4 and D-GalN, we did not observe a clear temporal trend of changes in the values of the tested markers (ALT, AST), which may be the result of the doses used, the regenerative capacity of the liver, and the 72-hour interval between the collection of the material for testing and last xenobiotic injection. The blood picture in the studied groups also did not show a specific trend of change. In humans, the increase in transaminase activity in CLD has only auxiliary diagnostic value. In the course of chronic liver injury, aminotransferase values are often normal and their significant increase suggests exacerbation of the disease [42]. Our previous studies show a strong upward trend

in the above-mentioned parameters during the first 48 hours after CCl_4 injection in rats and mice and D-GalN injection in rats (but not in mice) in the models of acute liver injury [43].

To sum up, the used doses of hepatotoxins allowed to show subtle differences in their effects over time, while avoiding too abrupt and advanced changes without the possibility of tracing intermediate stages. We assessed the severity of reversible and irreversible structural and functional changes in the liver in individual CLD models to determine the potentially optimal time of therapeutic intervention. Such CLD models might apply to different types of pharmaceutical treatments and to stem cell therapy. However, it should be noted that stem cell therapy has much more variables that might completely render the "timing" a less important limiting factor. For instance, the type of transplanted cells, their number, the pre-treatment/pre-genetic engineering of injected cells, the route of injection, the co-transplantation of more than one cell type, and many others are very powerful limiting factors that might influence its effectiveness. Based on this preclinical study, we can expect that in experimental rodents with established fibrosis large amount of collagen fibers which seal the sinusoids barrier, might prevent implanted cells homing process.

5. Conclusions

Summarizing the results obtained in the mouse and rat models using CCl_4, we can conclude that the dynamics of liver fibrosis in CCl_4 treated animals were greater than in the D-GalN groups.

In mice, and rats CCl_4 model we indicated two appropriate times for therapeutic intervention, which to varying degrees reflect the real clinical situation and may potentially differ in the obtained results: early intervention before week 4 of intoxication (during early fibrosis stage) and late intervention after week 8 of intoxication (when signs of established fibrosis are present).

We do not recommend rodent models of D-GalN-induced liver fibrosis due to the long incubation period, poor effect, and high costs.

Abbreviations

CCl_4, Carbon tetrachloride; D-GalN, D-galactosamine; CLD, chronic liver disease; i.p., intraperitoneal; ALT, alanine transaminase; AST, aspartate transaminase; ALP, alkaline phosphatase; TP, total protein; COL1A1, Type I collagen; COL3A1, Type III collagen; TGF-β, Transforming growth factor beta; c-Met, Tyrosine-protein kinase Met; HGF, Hepatocyte growth factor; CYP2E1, Cytochrome P450 2E1; PPAR-α, Peroxisome proliferator-activated receptor alpha.

Availability of Data and Materials

All data generated or analyzed during this study are included in this published article.

Author Contributions

PC and MK designed the research study. PC supported the studies financially (grands), provided help and advice. MK, EK, ŁL, AP, AS-S, EB, BS, MH, MM, AG, JP performed the research. PC, MK, ŁL, AS-S, BS, AP analyzed the data. PC and MK wrote the manuscript. All authors contributed to editorial changes in the manuscript. All authors read and approved the final manuscript.

Ethics Approval and Consent to Participate

Animal experiments were approved by the Animal Experiments Ethical Committee of Medical University of Silesia, Katowice, Poland (decision no. 18/2018).

Acknowledgment

We thank the Silesian Analytical Laboratory (Katowice; Poland) for performing serum biochemistry analysis and blood morphology assessment.

Funding

The studies were supported by institutional grants (SUM Katowice) no: KNW-1-103/N/8/0 and KNW-1-100/K/9/0.

Conflict of Interest

The authors declare no conflict of interest.

References

[1] Parola M, Pinzani M. Liver fibrosis: Pathophysiology, pathogenetic targets and clinical issues. Molecular Aspects of Medicine. 2019; 65: 37–55.

[2] Aydın MM, Akçalı KC. Liver fibrosis. The Turkish Journal of Gastroenterology. 2018; 29: 14–21.

[3] Roehlen N, Crouchet E, Baumert TF. Liver Fibrosis: Mechanistic Concepts and Therapeutic Perspectives. Cells. 2020; 9: 875.

[4] Castaldo ET, Chari RS. Liver transplantation for acute hepatic failure. HPB. 2006; 8: 29–34.

[5] Karvellas CJ, Francoz C, Weiss E. Liver Transplantation in Acute-on-chronic Liver Failure. Transplantation. 2021; 105: 1471–1481.

[6] Tsochatzis EA, Bosch J, Burroughs AK. Liver cirrhosis. Lancet. 2014; 383: 1749–1761.

[7] Andrewartha N, Yeoh G. Human Amnion Epithelial Cell Therapy for Chronic Liver Disease. Stem Cells International. 2019; 2019: 8106482.

[8] Miki T, Grubbs B. Therapeutic potential of placenta-derived stem cells for liver diseases: current status and perspectives. The Journal of Obstetrics and Gynaecology Research. 2014; 40: 360–368.

[9] Czekaj P, Król M, Limanówka Ł, Michalik M, Lorek K, Gramignoli R. Assessment of animal experimental models of toxic liver injury in the context of their potential application as preclinical models for cell therapy. European Journal of Pharmacology. 2019; 861: 172597.

[10] McGill MR, Jaeschke H. Animal models of drug-induced liver injury. Biochimica et Biophysica Acta. Molecular Basis of Disease. 2019; 1865: 1031–1039.
[11] Constandinou C, Henderson N, Iredale JP. Modeling liver fibrosis in rodents. Methods in Molecular Medicine. 2005; 117: 237–250.
[12] Bubnov RV, Drahulian MV, Buchek PV, Gulko TP. High regenerative capacity of the liver and irreversible injury of male reproductive system in carbon tetrachloride-induced liver fibrosis rat model. The EPMA Journal. 2017; 9: 59–75.
[13] Shi Y, Sun J, He H, Guo H, Zhang S. Hepatoprotective effects of Ganoderma lucidum peptides against D-galactosamine-induced liver injury in mice. Journal of Ethnopharmacology. 2008; 117: 415–419.
[14] Ganai AA, Husain M. Genistein attenuates D-GalN induced liver fibrosis/chronic liver damage in rats by blocking the TGF-β/Smad signaling pathways. Chemico-biological Interactions. 2017; 261: 80–85.
[15] Raafat N, Abdel Aal SM, Abdo FK, El Ghonaimy NM. Mesenchymal stem cells: In vivo therapeutic application ameliorates carbon tetrachloride induced liver fibrosis in rats. The International Journal of Biochemistry & Cell Biology. 2015; 68: 109–118.
[16] Ewida SF, Abdou AG, El-Rasol Elhosary AA, El-Ghane Metawe SA. Hepatocyte-like Versus Mesenchymal Stem Cells in CCl4-induced Liver Fibrosis. Applied Immunohistochemistry & Molecular Morphology. 2017; 25: 736–745.
[17] Lai L, Chen J, Wei X, Huang M, Hu X, Yang R, *et al*. Transplantation of MSCs Overexpressing HGF into a Rat Model of Liver Fibrosis. Molecular Imaging and Biology. 2016; 18: 43–51.
[18] Moriya K, Yoshikawa M, Ouji Y, Saito K, Nishiofuku M, Matsuda R, *et al*. Embryonic stem cells reduce liver fibrosis in CCl4-treated mice. International Journal of Experimental Pathology. 2008; 89: 401–409.
[19] Lin JS, Zhou L, Sagayaraj A, Jumat NHB, Choolani M, Chan JKY, *et al*. Hepatic differentiation of human amniotic epithelial cells and in vivo therapeutic effect on animal model of cirrhosis. Journal of Gastroenterology and Hepatology. 2015; 30: 1673–1682.
[20] Mamede KM, Sant'anna LB. Antifibrotic effects of total or partial application of amniotic membrane in hepatic fibrosis. Anais Da Academia Brasileira De Ciencias. 2019; 91: e20190220.
[21] Pietrosi G, Fernández-Iglesias A, Pampalone M, Ortega-Ribera M, Lozano JJ, García-Calderó H, *et al*. Human amniotic stem cells improve hepatic microvascular dysfunction and portal hypertension in cirrhotic rats. Liver International. 2020; 40: 2500–2514.
[22] Strom SC, Skvorak K, Gramignoli R, Marongiu F, Miki T. Translation of amnion stem cells to the clinic. Stem Cells and Development. 2013; 22 Suppl 1: 96–102.
[23] Strom SC, Gramignoli R. Human amnion epithelial cells expressing HLA-G as novel cell-based treatment for liver disease. Human Immunology. 2016; 77: 734–739.
[24] Batts KP, Ludwig J. Chronic hepatitis. An update on terminology and reporting. The American Journal of Surgical Pathology. 1995; 19: 1409–1417.
[25] Goodman ZD. Grading and staging systems for inflammation and fibrosis in chronic liver diseases. Journal of Hepatology. 2007; 47: 598–607.
[26] Bingül İ, Aydın AF, Başaran-Küçükgergin C, Doğan-Ekici I, Çoban J, Doğru-Abbasoğlu S, *et al*. High-fat diet plus carbon tetrachloride-induced liver fibrosis is alleviated by betaine treatment in rats. International Immunopharmacology. 2016; 39: 199–207.
[27] Schindelin J, Arganda-Carreras I, Frise E, Kaynig V, Longair M, Pietzsch T, *et al*. Fiji: an open-source platform for biological-image analysis. Nature Methods. 2012; 9: 676–682.
[28] Standish RA, Cholongitas E, Dhillon A, Burroughs AK, Dhillon AP. An appraisal of the histopathological assessment of liver fibrosis. Gut. 2006; 55: 569–578.
[29] Krishna M. Histological Grading and Staging of Chronic Hepatitis. Clinical Liver Disease. 2021; 17: 222–226.
[30] Rich L, Whittaker P. Collagen and Picrosirius Red Staining: A polarized light assessment of fibrillar hue and spatial distribution. Journal of Morphological Sciences. 2005; 22: 97–104.
[31] Gibson-Corley KN, Olivier AK, Meyerholz DK. Principles for valid histopathologic scoring in research. Veterinary Pathology. 2013; 50: 1007–1015.
[32] Bai Q, Yan H, Sheng Y, Jin Y, Shi L, Ji L, *et al*. Long-term acetaminophen treatment induced liver fibrosis in mice and the involvement of Egr-1. Toxicology. 2017; 382: 47–58.
[33] Giebeler A, Boekschoten MV, Klein C, Borowiak M, Birchmeier C, Gassler N, *et al*. c-Met confers protection against chronic liver tissue damage and fibrosis progression after bile duct ligation in mice. Gastroenterology. 2009; 137: 297–308, 308.e1–308.e4.
[34] Vasir B, Reitz P, Xu G, Sharma A, Bonner-Weir S, Weir GC. Effects of diabetes and hypoxia on gene markers of angiogenesis (HGF, cMET, uPA and uPAR, TGF-alpha, TGF-beta, bFGF and Vimentin) in cultured and transplanted rat islets. Diabetologia. 2000; 43: 763–772.
[35] Sutti S, Rigamonti C, Vidali M, Albano E. CYP2E1 autoantibodies in liver diseases. Redox Biology. 2014; 3: 72–78.
[36] Montagner A, Polizzi A, Fouché E, Ducheix S, Lippi Y, Lasserre F, *et al*. Liver PPARα is crucial for whole-body fatty acid homeostasis and is protective against NAFLD. Gut. 2016; 65: 1202–1214.
[37] Hong L, Sun QF, Xu TY, Wu YH, Zhang H, Fu RQ, *et al*. New role and molecular mechanism of Gadd45a in hepatic fibrosis. World Journal of Gastroenterology. 2016; 22: 2779–2788.
[38] Karp JM, Leng Teo GS. Mesenchymal stem cell homing: the devil is in the details. Cell Stem Cell. 2009; 4: 206–216.
[39] Mohamadnejad M, Alimoghaddam K, Mohyeddin-Bonab M, Bagheri M, Bashtar M, Ghanaati H, *et al*. Phase 1 trial of autologous bone marrow mesenchymal stem cell transplantation in patients with decompensated liver cirrhosis. Archives of Iranian Medicine. 2007; 10: 459–466.
[40] Mito M, Kusano M. Hepatocyte Transplantation in Man. Cell Transplantation. 1993; 2: 65–74.
[41] Zhao Y, Ye W, Wang YD, Chen WD. HGF/c-Met: A Key Promoter in Liver Regeneration. Frontiers in Pharmacology. 2022; 13: 808855.
[42] Bajaj JS, O'Leary JG, Lai JC, Wong F, Long MD, Wong RJ, *et al*. Acute-on-Chronic Liver Failure Clinical Guidelines. The American Journal of Gastroenterology. 2022; 117: 225–252.
[43] Czekaj P, Król M, Limanówka Ł, Skubis-Sikora A, Kolanko E, Bogunia E, *et al*. Dynamics of Acute Liver Injury in Experimental Models of Hepatotoxicity in the Context of Their Implementation in Preclinical Studies on Stem Cell Therapy. Frontiers in Bioscience-Landmark. 2022; 27: 237.
[44] Fujita T, Narumiya S. Roles of hepatic stellate cells in liver inflammation: a new perspective. Inflammation and Regeneration. 2016; 36: 1.
[45] Hamdi S, Abdel Salam H. Curative Effect of Dietary Freshwater and Marine Crustacean Extracts on Carbon Tetrachloride-induced Nephrotoxicity. Australian Journal of Basic and Applied Sciences. 2009; 3: 2118–2129.
[46] Knockaert L, Berson A, Ribault C, Prost PE, Fautrel A, Pajaud J, *et al*. Carbon tetrachloride-mediated lipid peroxidation induces early mitochondrial alterations in mouse liver. Laboratory Investigation. 2012; 92: 396–410.
[47] Tierney DJ, Haas AL, Koop DR. Degradation of cytochrome P450 2E1: selective loss after labilization of the enzyme.

Archives of Biochemistry and Biophysics. 1992; 293: 9–16.
[48] Nakajima M, Iwata K, Yamamoto T, Funae Y, Yoshida T, Kuroiwa Y. Nicotine metabolism in liver microsomes from rats with acute hepatitis or cirrhosis. Drug Metabolism and Disposition: the Biological Fate of Chemicals. 1998; 26: 36–41.
[49] Osawa Y, Nagaki M, Banno Y, Yamada Y, Imose M, Nozawa Y, *et al*. Possible involvement of reactive oxygen species in D-galactosamine-induced sensitization against tumor necrosis factor-alpha-induced hepatocyte apoptosis. Journal of Cellular Physiology. 2001; 187: 374–385.
[50] Schattenberg JM, Czaja MJ. Regulation of the effects of CYP2E1-induced oxidative stress by JNK signaling. Redox Biology. 2014; 3: 7–15.
[51] Decker K, Keppler D. Galactosamine hepatitis: key role of the nucleotide deficiency period in the pathogenesis of cell injury and cell death. Reviews of Physiology, Biochemistry and Pharmacology. 1974; 77–106.
[52] Kumar S, Duan Q, Wu R, Harris EN, Su Q. Pathophysiological communication between hepatocytes and non-parenchymal cells in liver injury from NAFLD to liver fibrosis. Advanced Drug Delivery Reviews. 2021; 176: 113869.
[53] Tsuchida T, Friedman SL. Mechanisms of hepatic stellate cell activation. Nature Reviews. Gastroenterology & Hepatology. 2017; 14: 397–411.
[54] Mortezaee K, Khanlarkhani N, Sabbaghziarani F, Nekoonam S, Majidpoor J, Hosseini A, *et al*. Preconditioning with melatonin improves therapeutic outcomes of bone marrow-derived mesenchymal stem cells in targeting liver fibrosis induced by CCl4. Cell and Tissue Research. 2017; 369: 303–312.
[55] Khanjarsim V, Karimi J, Khodadadi I, Mohammadalipour A, Goodarzi MT, Solgi G, *et al*. Ameliorative Effects of Nilotinib on CCl4 Induced Liver Fibrosis Via Attenuation of RAGE/HMGB1 Gene Expression and Oxidative Stress in Rat. Chonnam Medical Journal. 2017; 53: 118–126.
[56] Beljaars L, Daliri S, Dijkhuizen C, Poelstra K, Gosens R. WNT-5A regulates TGF-β-related activities in liver fibrosis. American Journal of Physiology. Gastrointestinal and Liver Physiology. 2017; 312: G219–G227.
[57] Ji DG, Zhang Y, Yao SM, Zhai XJ, Zhang LR, Zhang YZ, *et al*. Cav-1 deficiency promotes liver fibrosis in carbon tetrachloride (CCl_4)-induced mice by regulation of oxidative stress and inflammation responses. Biomedicine & Pharmacotherapy. 2018; 102: 26–33.
[58] Shi Z, Wakil AE, Rockey DC. Strain-specific differences in mouse hepatic wound healing are mediated by divergent T helper cytokine responses. Proceedings of the National Academy of Sciences of the United States of America. 1997; 94: 10663–10668.
[59] Jiang W, Tan Y, Cai M, Zhao T, Mao F, Zhang X, *et al*. Human Umbilical Cord MSC-Derived Exosomes Suppress the Development of CCl_4-Induced Liver Injury through Antioxidant Effect. Stem Cells International. 2018; 2018: 6079642.
[60] Gressner OA, Weiskirchen R, Gressner AM. Biomarkers of hepatic fibrosis, fibrogenesis and genetic pre-disposition pending between fiction and reality. Journal of Cellular and Molecular Medicine. 2007; 11: 1031–1051.
[61] Xu F, Liu C, Zhou D, Zhang L. TGF-β/SMAD Pathway and Its Regulation in Hepatic Fibrosis. The Journal of Histochemistry and Cytochemistry. 2016; 64: 157–167.
[62] Ganai AA, Ganaie IA, Verma N, Farooqi H. Regression of fibrosis/cirrhosis by Glycine propionyl-l-carnitine treatment in d-Galactosamine induced chronic liver damage. Chemico-biological Interactions. 2016; 260: 117–128.
[63] Chowdhury AB, Mehta KJ. Liver biopsy for assessment of chronic liver diseases: a synopsis. Clinical and Experimental Medicine. 2022. (online ahead of print)
[64] Oakley F, Trim N, Constandinou CM, Ye W, Gray AM, Frantz G, *et al*. Hepatocytes express nerve growth factor during liver injury: evidence for paracrine regulation of hepatic stellate cell apoptosis. The American Journal of Pathology. 2003; 163: 1849–1858.
[65] Vernon G, Baranova A, Younossi ZM. Systematic review: the epidemiology and natural history of non-alcoholic fatty liver disease and non-alcoholic steatohepatitis in adults. Alimentary Pharmacology & Therapeutics. 2011; 34: 274–285.
[66] Cramer T, Schuppan D, Bauer M, Pfander D, Neuhaus P, Herbst H. Hepatocyte growth factor and c-Met expression in rat and human liver fibrosis. Liver International. 2004; 24: 335–344.
[67] Jonker AM, Dijkhuis FW, Hardonk MJ, Moerkerk P, Ten Kate J, Grond J. Immunohistochemical study of hepatic fibrosis induced in rats by multiple galactosamine injections. Hepatology. 1994; 19: 775–781.
[68] Tsuji T, Shinohara T. Pathological study of chronic D-galactosamine induced hepatitis in mice by administration of adjuvants - an animal model of the chronic active hepatitis. Gastroenterologia Japonica. 1981; 16: 9–20.
[69] Catal T, Bolkent S. Combination of selenium and three naturally occurring antioxidants administration protects D-galactosamine-induced liver injury in rats. Biological Trace Element Research. 2008; 122: 127–136.
[70] Tsutsui S, Hirasawa K, Takeda M, Itagaki S, Kawamura S, Maeda K, *et al*. Apoptosis of murine hepatocytes induced by high doses of galactosamine. The Journal of Veterinary Medical Science. 1997; 59: 785–790.